THERMAL PROTECTION CONCEPTS FOR MOBILE AND DUSTY LUNAR EXPERIMENTS

by

RICHARD JAY LANGLEY

B.S., Virginia Polytechnic Institute, 1970

Submitted in Partial Fulfillment

of the Requirements for the Degree of

MASTER OF SCIENCE

at the

Massachusetts Institute of Technology

September 1971

Signature of Author _____

Department of Aeronautics and Astronautics

Certified by _____

Thesis Supervisor

Accepted by _____

Chairman, Departmental Committee on Graduate Students

THERMAL PROTECTION CONCEPTS FOR MOBILE AND DUSTY LUNAR EXPERIMENTS

by

Richard Jay Langley

Submitted to the Department of Aeronautics and Astronautics on June 28, 1971 in partial fulfillment of the requirements for the degree of Master of Science in Aeronautics and Astronautics.

ABSTRACT

A passive thermal protection concept is developed that improves the thermal performance of simple radiative surfaces in mobile, dusty, lunar environments. The concept consists of secondary surfaces which shade the primary surface at high solar elevations, thus lowering the maximum temperatures incurred. At low solar elevations, the secondary blocks radiation from the primary surface and thereby raises its minimum temperature. Optimization parameters for dual surface configurations are illustrated.

Several methods of raising the minimum temperature of the primary surface at low solar elevations are discussed, including solar powered heaters, variable area primary surfaces, glass covered high absorptance materials, and conical secondaries. Various means of lowering the maximum temperatures incurred by the basic dual surface design are described, including multi-characteristic materials, conical secondary surfaces, and infrared radiation shields.

Thesis Supervisor: Professor John V. Harrington
Department of Aeronautics and Astronautics

ACKNOWLEDGEMENTS

I wish to express my sincere gratitude to Mr. R. H. Baker for his helpful guidance and unselfish contribution of time and ideas while acting as my immediate supervisor, and to Dr. J. V. Harrington who was my thesis advisor. I would also like to thank the MIT Center for Space Research and Dr. Gene Simmons, whose support made this work possible.

Ved Nanda deserves a particular note of appreciation for his helpful criticisms, as does Miss Mary De Sesa who helped in typing. Finally, but possibly most important, I wish to thank the girls next door for putting up with me...

TABLE OF CONTENTS

LIST OF FIGURES

LIST OF TABLES

SYMBOLS

A_1 - area of the primary surface

A_{1x} - unshaded area of the primary surface

A_2 - area of the secondary surface

A_{2B} - area of the bottom of the secondary surface

A_{2T} - area of the top of the secondary surface

A_{2x} - area of the secondary surface exposed to lunar albedo

A_L - area of the lunar surface

D_1 - diameteter of the primary surface

D_2 - diameter of the secondary surface

F_{ij} - geometric view factor representing the fraction of energy radiated by surface i that is incident on surface j. Subscripts i and j follow the same definitions as those for area, above.

G - solar constant

H - height of the secondary surface

H_p - height of the solar panel

k_{ij} - ratio of area j to area i

L - apparent displacement of two surface due to solar elevation

P - internal power dissipation

R_1 - radius of the primary surface

R_2 - radius of the secondary surface

R_{2B} - radius of the bottom of a conical secondary surface

R_{2T} - radius of the top of a conical secondary surface

α_s - solar absorptance; numerical subscritps refer to surface defined for areas

β - angle between the side of a conical secondary and the horizontal

ε - emittance; numerical subscripts refer to surfaces defined for areas

σ - Stefan-Boltzman constant

τ_V - transmittance in visible light spectrum

τ_{IR} - transmittance in the infrared light spectrum

Θ - solar elevation

CHAPTER 1

INTRODUCTION

The concepts of thermal protection developed in this thesis are the result of work relating to the design of the Surface Electrical Properties (SEP) experiment scheduled to be flown on the Apollo 17 mission in 1972. The SEP receiver assembly is mobile, dissipates 6.5 watts of power internally, and includes a tape recorder which must be maintained between 5°C and 50°C during operation. Lunar surface temperatures, on the other hand, range from -175°C at night, through -60°C at dawn, up to 125°C at lunar noon.

Design of a lightweight thermal protection system that satisfies the above requirements is complicated by lunar dust, which degrades radiative surfaces, and the fact that the SEP receiver is mobile, which causes the solar orientation to change in both azimuth and elevation with respect to the radiative surface of the experimental package. In addition, the sun passes from horizon to horizon at the rate of .5°/hour. Azimuth and elevation are defined in Figure 1.1.

Contamination from lunar dust causes degradation of radiative surfaces used in thermal protection systems. The NASA Manned Space Center has some preliminary information about how the properties of various materials change with dust conditions, and the results indicate that degradation of radiative surfaces causes the solar absorptance and the emittance to

change and ultimately approach the values of the lunar surface (α_s = .90, ε = .85). In this thesis, second surface mirrors are used for the radiative surfaces which will be assumed to degrade with dust according to the values given in Table 1.1.

TABLE 1.1 - CLEAN AND DEGRADED VALUES USED FOR SECOND SURFACE MIRRORS

Contamination	α_s	ε
none (clean)	.085	.85
dusty	.20	.85
very dusty	.40	.85
dirty	.90	.85

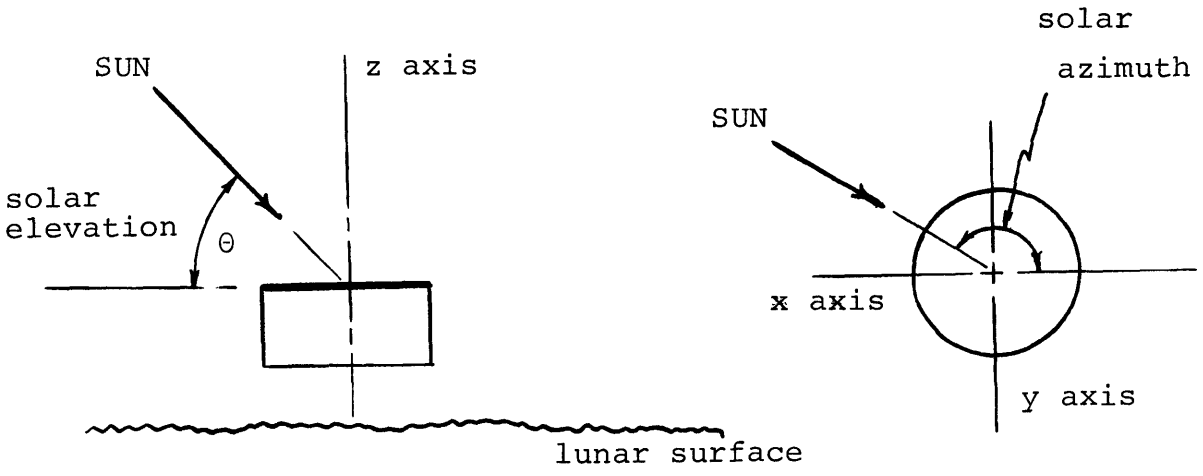

Figure 1.1 - Azimuth and Elevation

CHAPTER 2

FUNDAMENTALS OF SIMPLE RADIATIVE SURFACES

2.1 Equilibrium Equations

The basic thermal model for an experiment dissipating power through a radiative surface is shown in Figure 2.1. The equilibrium equation for this configuration may be written as:

$$\begin{bmatrix}\text{energy}\\ \text{radiated}\end{bmatrix} = \begin{bmatrix}\text{internal power}\\ \text{dissipation}\end{bmatrix} + \begin{bmatrix}\text{solar energy}\\ \text{absorbed}\end{bmatrix}$$

$$\sigma\varepsilon T^4 A = P + G\alpha_s A \sin(\theta) \quad (2.1)$$

where G = solar flux (130 watts/ft^2)

P = internal power dissipation (watts)

σ = Stefan-Boltzmann Constant ($.527 \times 10^{-8}$ $\frac{\text{watts}}{\text{ft}^2\text{-}(^\circ\text{K})^4}$)

α_s = solar absorptance of radiative surface (see Table 1.1)

ε = emittance of radiative surface (.85)

A = area of radiative surface (ft^2)

θ = solar elevation

T = equilibrium temperature of radiative surface (°K)

2.2 Performance of Simple Radiative Surface and Comparison to SEP Requirements

The temperature of the radiating surface of the basic model as a function of sun elevation and surface conditions is shown in Figures 2.2A and 2.2B for two different ratios of P/A. Equation 2.1 was used to generate these curves.

The minimum and maximum allowable temperature for the SEP experiment is 5°C and 50°C respectively. The results of

Figures 2.2A and 2.2B indicate that in order to meet the SEP experiment thermal requirements it is necessary, as indicated qualitatively in Figure 2.3, to both raise the temperature of the basic model at low sun elevations and lower it at high sun elevations. The following chapters develop concepts which achieve these goals.

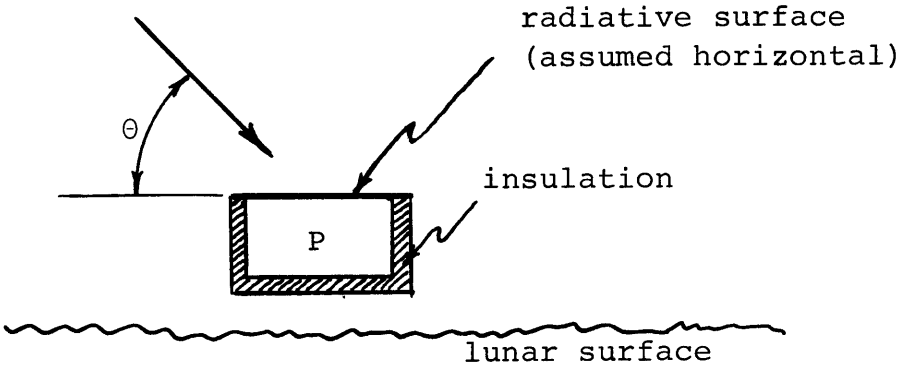

Figure 2.1 - Basic Model for Lunar Experiment with Simple Radiative Surface

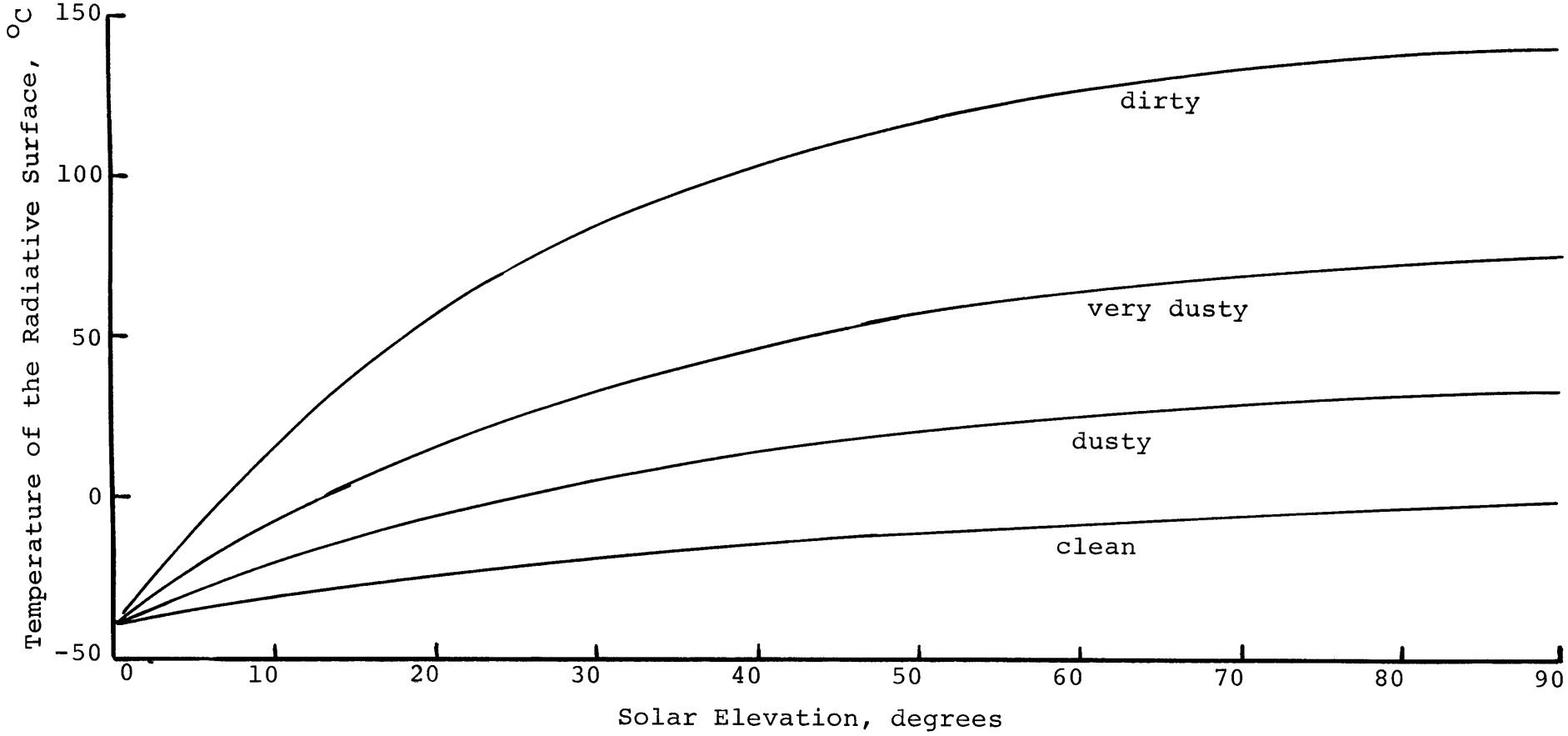

Figure 2.2A - P/A = 13 watt/ft^2

Figure 2.2 - Thermal Performance of Single Radiative Surface Model

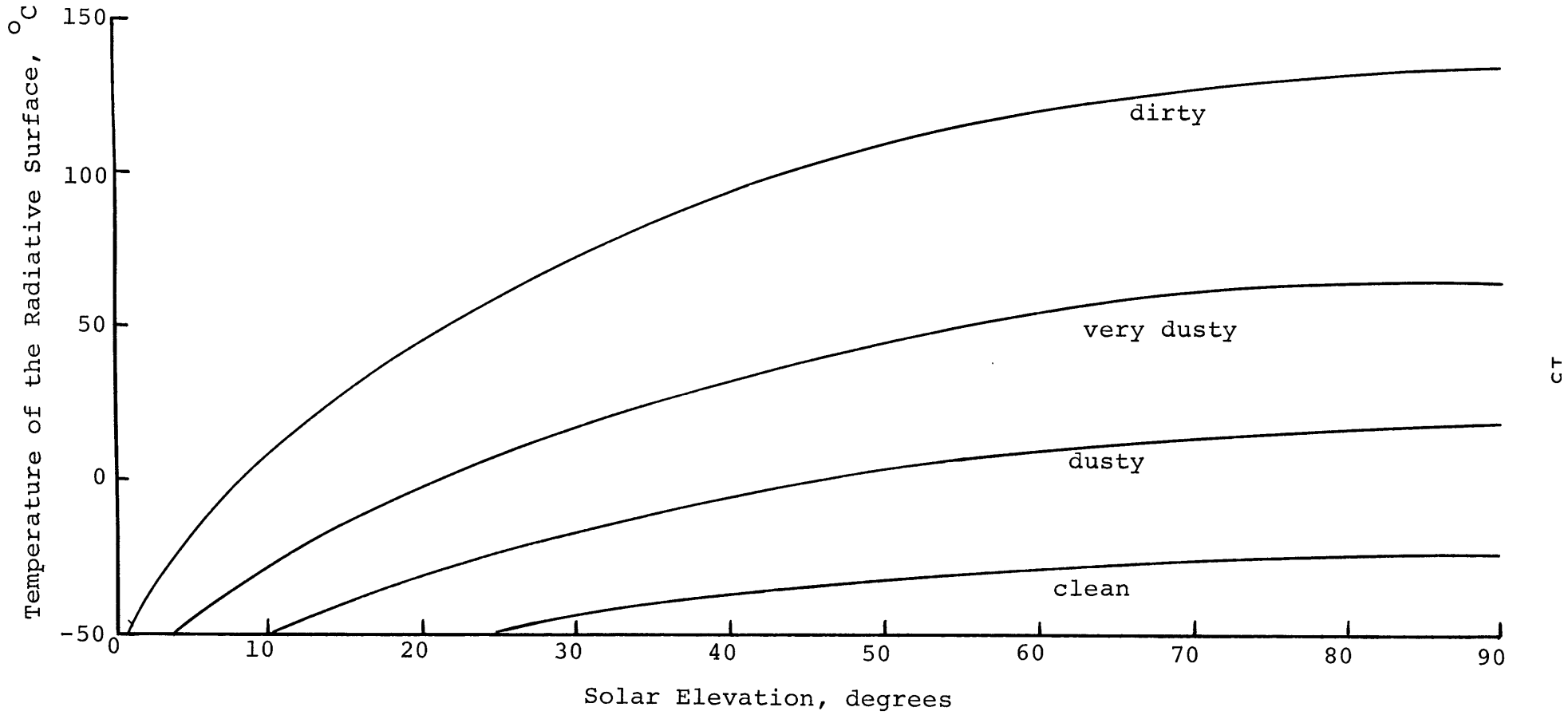

Figure 2.2B - P/A = 6.5 watt/ft^2

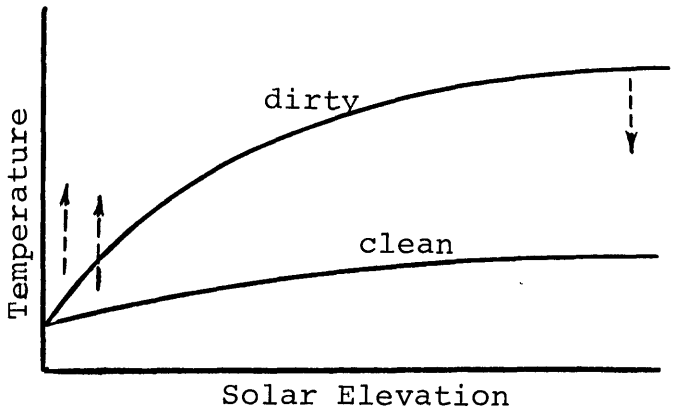

LEGEND

-solid curves represent thermal performance of a single surface design

-dotted arrows represent desired improvement of single surface design

Figure 2.3 - Thermal Performance of Basic Single Surface Model With Desired Improvements

CHAPTER 3

PLANAR DUAL SURFACE SYSTEMS

3.1 General

A planar dual surface configuration will improve the thermal performance of the simple radiative surface model of Figure 2.1. The basic model for the dual surface design consists of two parallel flat surfaces as shown in Figure 3.1. In this chapter, only flat plate secondary surfaces are discussed while chapter 4 considers more complex secondary geometries.

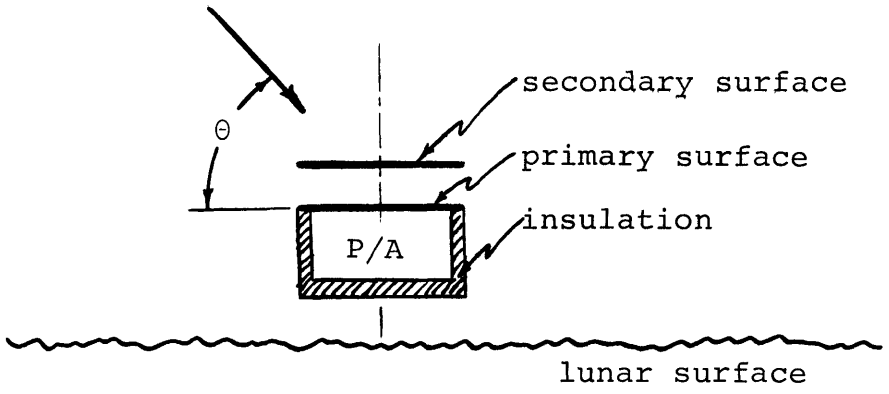

Figure 3.1 - Basic Model for Lunar Experiment with Dual Surface Configuration

3.2 Theoretical Basis for the Dual Surface Concept

A comparison between the single and dual surface models will be made in order to determine the relative thermal performance of the two configurations at high and low sun elevations. The approach used in this comparison is to

instantaneously create a second surface above the original single surface and examine the energy transfer from both surfaces to the surrounding medium at the instant of transition from single surface to dual surface design. For convenience, the energy transfers for the primary surface are based on the assumption that the temperature of the secondary is initially at the same temperature as the primary surface (see Figure 3.2). The temperature of the secondary is then shown to be consistent with thethermal inequalities shown for the primary surface.

3.2.1 Low Solar Elevations

Consider the basic model with a single radiative surface (Figure 2.1) at zero degrees solar elevation. No solar energy is incident on either the lunar surface or the radiating surface, thus the discussion at this elevation is independent of the surface degradation of the configuration. Because the radiating surface is dissipating internal power, $T_1 > T_L$ where T_1 is the radiating surface equilibrium temperature and T_L is the lunar surface temperature.

The energy transfers for a dual surface configuration at time t_1 are shown in Figure 3.3. Referring to Figures 3.2 and 3.3, it is known that $q_a = q_c + q_d$ at time t_o because there is no absorption of solar energy. At time t_1 the primary surface of the dual surface model radiates the same quantity of energy, since it is still at temperature T_1. There are only four components of energy transfer for the primary surface: q_a, q_b, q_c, and q_d. It is known that at time t_o, $q_a = q_c + q_d$

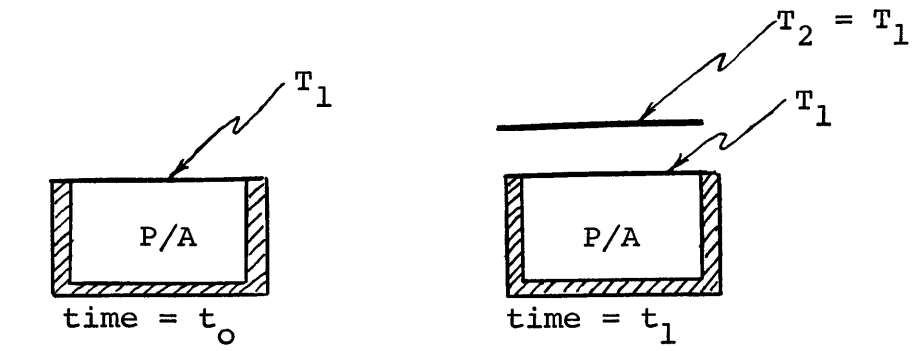

single surface model

dual surface model

$$t_1 - t_o \to 0$$

Figure 3.2 - Instantaneous Transition From Single Surface to Dual Surface Model

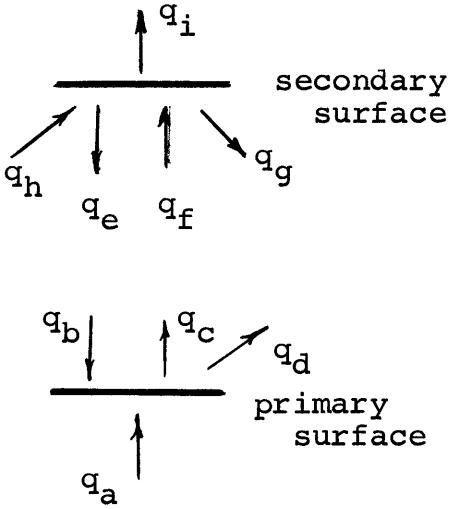

q_a = internal power dissipation

q_b = infrared radiation (IR) absorbed from secondary

q_c = IR radiated to secondary

q_d = IR radiated to space

q_e = IR radiated to primary

q_f = IR absorbed from primary

q_g = IR radiated to lunar surface

q_h = IR absorbed from lunar surface

q_i = IR radiated to space

Figure 3.3 - Energy Transfers for Dual Surface Model at Instant of Transition

and that $q_b > 0$. Thus the inequality $q_a + q_b > q_c + q_d$ follows, and therefore, the primary surface absorbs more energy than it is emitting. Thus, the primary surface must heat in reaching a new equilibrium. This is true for any finite temperature of the secondary surface.

For the secondary surface, $q_e = q_f$ since $T_1 = T_2$ at time t_1, Also, as noted previously, $T_2 > T_L$ and hence $q_g > q_h$. In addition, $q_i > 0$ and therefore a net energy transfer occurs to space and the lunar surface. Thus, the secondary must cool in reaching a new equilibrium.

Net energy transfers for primary and secondary surfaces at time t_1, with zero degree solar elevation, are shown in Figure 3.4.

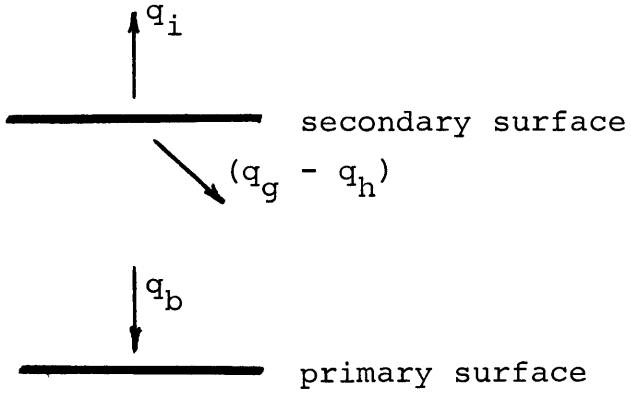

Figure 3.4 - Net Energy Transfers for Dual Surface Model at Time t_1, Zero Degree Solar Elevation

3.2.2 High Solar Elevations

The radiative surfaces of the single surface and dual surface models absorb solar energy at high sun elevations. The theoretical development of this section will consider the two limiting cases of solar absorptance for these surfaces: that is, (1) completely contaminated surfaces with high solar absorptance, and (2) clean surfaces with very low solar absorptance.

3.2.2.1 Dirty Surface Conditions

Again consider the instantaneous transition from a single surface model into a dual surface model. Under dirty conditions, the single surface has characteristics identical to the lunar surface. Since $P/A > 0$ we know that at time t_1 $T_1 = T_2 > T_L$. Figure 3.5 shows the energy transfers for both surfaces at time t_1, where q_a through q_i are defined as in Figure 3.3 and q_j is the solar energy absorbed by the secondary.

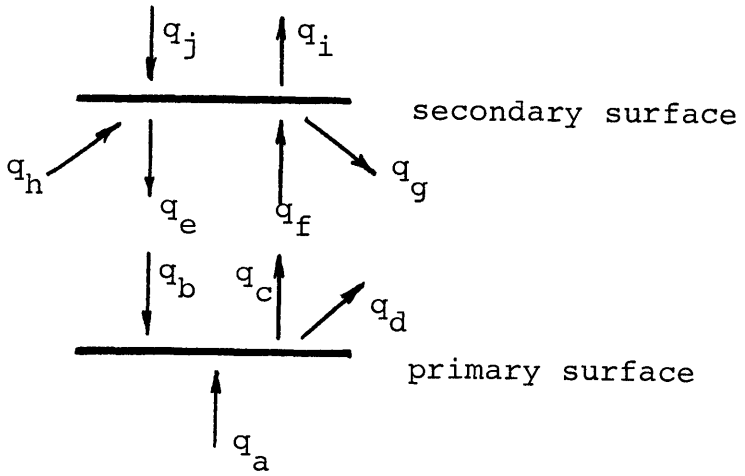

Figure 3.5 - Energy Transfers for Dual Surface Model at Time t_1, Dirty Conditions

Consider the primary surface of Figure 3.5. If the separation of the surfaces approaches zero, then $q_d \rightarrow 0$ such that q_c becomes the total emitted energy from the primary and q_b equals the solar absorption. This is consistent with the single surface (separation = 0) equilibrium equation

$$q_a + q_b = q_c + q_d \quad \text{where } q_d = 0$$

As the separation is increased, q_d becomes larger, i.e. the primary "sees" more space. In addition, q_b becomes smaller because some of the emitted energy from the secondary is no longer incident on the primary surface. (Note that we are assured of this only if the temperature of the secondary does not increase after separation to compensate for the decreased coupling of the two surfaces. The following paragraph demonstrates that the secondary actually cools.) With q_d increasing with separation, and q_b decreasing, the above equation becomes an inequality

$$q_a + q_b < q_c + q_d$$

The energy absorbed is less than the energy emitted at time t_1 and the primary must cool in reaching a new equilibrium.

For the secondary surface of Figure 3.5, $q_e = q_f$ because $T_1 = T_2$, and $q_h < q_g$ since $T_2 > T_L$. It can be shown that $q_i > q_j$ by examining the single surface equilibrium condition:

$$\begin{bmatrix}\text{energy}\\ \text{radiated}\end{bmatrix} = \begin{bmatrix}\text{solar energy}\\ \text{absorbed}\end{bmatrix} + \begin{bmatrix}\text{internal power}\\ \text{dissipation}\end{bmatrix}$$

$$q_i = q_j + q_a$$

Thus, $q_i > q_j$ for P/A > 0. At the instant of transition, there is a net energy transfer to space and the lunar surface, thus the secondary must cool in reaching a new equilibrium.

The net energy transfers for primary and secondary surfaces at the time of transition are shown in Figure 3.6.

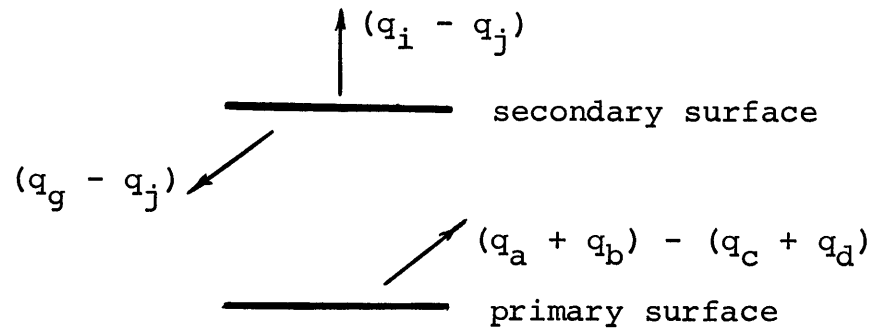

Figure 3.6 - Net Energy Transfers for Dual Surface Model, Dirty Conditions

3.2.2.2 Super-Clean Surface Conditions

Although the minimum $\frac{\alpha}{\varepsilon}$ ratio concerning this thesis is assumed to be .10, it is convenient to define a "super-clean" surface with $\frac{\alpha_s}{\varepsilon} = 0$ for purposes of conceptually developing the dual surface model. Such a surface absorbs no solar energy ($\alpha_s = 0$), but does absorb IR radiation ($\varepsilon = .85$). At 90° solar elevation, the equilibrium of the single surface model will

depend solely on the P/A ratio. Any desired temperature may be achieved by increasing or decreasing the radiative surface area of the model. For practical cases, where it is required to protect electronics or sensitive components from excessive temperatures, desireable temperatures will be less than 125°C. At $\theta = 90°$ this means $T_1 < T_L$. Energy transfers for primary and secondary surfaces are defined as in Figure 3.5. The only difference between the anlysis of super-clean and dirty surfaces is the value of solar absorptance and the fact that $T_1 < T_L$.

For the primary surface of the dual surface model, we know that $q_a = q_c + q_d$ (no absorption of solar energy). Since $q_b > 0$, there is a net energy transfer into the primary and the primary surface must heat in reaching a new equilibrium.

For the secondary surface $q_j = 0$ and $q_e = q_f$. Because $T_2 < T_L$, q_g F q_h. Also, $q_i > 0$. The quantity $(q_h - q_g)$ is dependent on the separation of the plates, and the temperature T_2. Since T_2 is dependent solely on P/A, the change in secondary surface temperature is dependent on separation and P/A.

Mathematically,

$$q_i = \sigma \varepsilon_2 T_2^4 A_2 = P \quad \text{(single surface equilibrium equation)} \qquad (3.1)$$

and $(q_h - q_g) = \sigma\varepsilon_L(T_L^4 - T_2^4)F_{2L}A_2\varepsilon_2$

where ε_L = emittance of lunar surface (.85)

ε_2 = emittance of secondary surface ($\varepsilon_2 = \varepsilon_L$)

T_2 = temperature of secondary surface

T_L = temperature of lunar surface

A_2 = area of secondary surface

F_{2L} = geometric view factor representing fraction of energy emitted from secondary that is incident on lunar surface

Assuming that the lunar surface temperature may be approximated by

$$T_L = \sqrt[4]{\frac{G\alpha_L \sin(\theta)}{\sigma\varepsilon_L}}$$

where α_L is the solar absorptance of the lunar surface

then $(q_h - q_g) = (G\alpha_L - P/A)F_{2L}A\varepsilon_2$

The secondary heats for

$q_i < (q_h - q_g)$ which may be rewritten using equations 3.1 and 3.2.

$$P < (G\alpha_L - P/A)F_{2L}A\varepsilon_2$$

$$P/A < \frac{G\alpha_L F_{2L}\varepsilon_2}{1 + F_{2L}\varepsilon_2} \qquad (3.3)$$

Equation 3.3 is true for small values of the ratio P/A, provided the view factor F_{2L} does not approach zero. It holds for all configurations discussed later on. For example, the following parameters typically apply to configurations developed later in this thesis.

$$P/A = 6.5 \text{ wt/ft}^2$$

$$G = 130 \text{ wt/ft}^2$$

$$F_{2L} = .55$$

$$\varepsilon_2 = \varepsilon_L = .85$$

$$\alpha_L = .90$$

These values result in the inequality 6.5 <35, which is in agreement with equation 3.3, thus the secondary heats in reaching a new equilibrium.

Net energy transfers for primary and secondary surfaces at the instant of transition are shown in Figure 3.7.

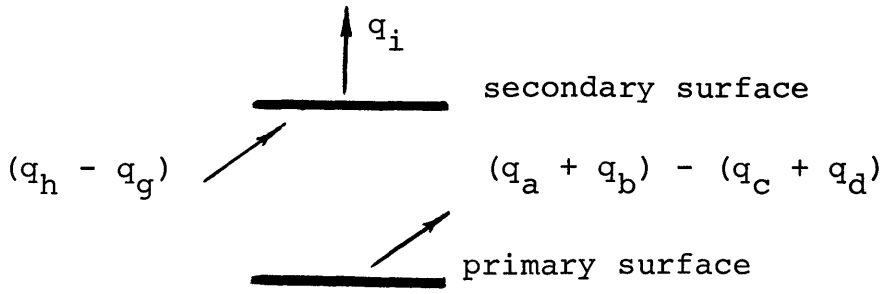

Figure 3.7 - Net Energy Transfers for Dual Surface Model, Super-Clean Conditions

3.2.3 Summary

It has been shown that at low sun elevations the dual surface design raises the primary surface temperature relative to that of the single surface model. At high sun elevations the dual surface design lowers the primary surface temperature for dirty conditions and raises the temperature for clean conditions relative to the single surface model. The qualitative results as shown in Figure 3.8 are desirable in terms of the objectives stated earlier which were to raise temperatures at low sun elevations, and lower temperatures at high sun elevations.

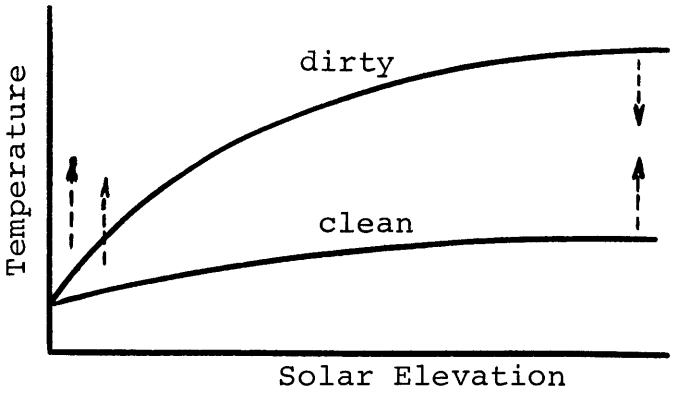

LEGEND

-solid curves represent thermal performance of a single surface design

-dotted arrows represent effect of adding a secondary surface to a single surface design

Figure 3.8 - Qualitative Improvement of Dual Surface Model Relative to Single Surface Model

3.3 Dual Surface Performance

This section develops the basic thermal equilibrium equations for the dual surface configuration, which are used to numerically demonstrate the thermal performance of several examples.

3.3.1 Assumptions for Equations

Six assumptions are made in developing the equilibrium equations:

1) The insulation on the sides and bottom of the experiment package is perfect (no energy transfer through the insulation).
2) All surfaces are isothermal.
3) All surfaces are diffuse (Lambert's Cosine law).

4) Most IR radiation is absorbed by the surface it is incident upon and a large fraction of the remainder is reflected away from the configuration. This is a close approximation because we are dealing with high emittance surfaces and geometric view factors not near one.

5) Lunar albedo is diffuse. For purposes of computation, albedo is included in the lunar IR term. This is acceptable, because in the configurations to be considered, it yields a conservative estimate of thermal performance.

6) The primary radiative surface is assumed to remain level with respect to the lunar horizon, and the lunar surface is assumed to be flat. This allows solar elevation to be measured relative to either the experiment package or the lunar horizon. It also allows the lunar surface temperature to be calculated as a simple function of solar elevation.

3.3.2 Thermal Equilibrium Equations

The equilibrium equations for the dual surface configuration of Figure 3.1 may be written as follows.

Equilibrium of the primary surface:

$$\begin{bmatrix}\text{energy}\\ \text{radiated}\end{bmatrix} = \begin{bmatrix}\text{solar energy}\\ \text{absorbed}\end{bmatrix} + \begin{bmatrix}\text{internal}\\ \text{dissipation}\end{bmatrix} + \begin{bmatrix}\text{secondary IR}\\ \text{absorbed}\end{bmatrix} \tag{3.1}$$

$$\sigma\varepsilon_1 A_1 T_1^4 = G\alpha_{s1}\sin(\theta)A_{1x} + P + \sigma\varepsilon_2 A_2 F_{21} T_2^4 \varepsilon_1 \tag{3.2}$$

Equilibrium of the secondary surface:

$$\begin{bmatrix}\text{energy radiated}\\ \text{(both sides)}\end{bmatrix} = \begin{bmatrix}\text{direct solar}\\ \text{energy absorbed}\end{bmatrix} + \begin{bmatrix}\text{solar energy}\\ \text{reflected from}\\ \text{primary surface}\end{bmatrix} + \begin{bmatrix}\text{lunar albedo}\\ \text{absorbed}\end{bmatrix} + \begin{bmatrix}\text{lunar IR}\\ \text{absorbed}\end{bmatrix} + \begin{bmatrix}\text{IR from primary}\\ \text{surface absorbed}\end{bmatrix} \tag{3.3}$$

$$\sigma\varepsilon_2 {}^2A_2 T_2^4 = G\alpha_{s2}\sin(\theta)A_2 + G(1-\alpha_{s1})\sin(\theta)A_{1x} + G(1-\alpha_L)\sin(\theta)A_{2x} + \sigma\varepsilon_L A_L F_{L2} T_L^4 \varepsilon_2 + \sigma\varepsilon_1 A_1 F_{12} T_1^4 \varepsilon_2 \tag{3.4}$$

where A_{1x} = the unshaded area of the primary surface (see Appendix A)

A_{2x} = the area of the secondary exposed to lunar albedo (not used in numerical computations since albedo is included in lunar IR term)

F_{12}, F_{21}, and F_{2L} are geometric view factors calculated as follows (see Reference 4).

$$F_{12} = 1/2 \left(x - \sqrt{x^2 - 4E^2D^2}\right) \tag{3.5}$$

$$x = 1 + (1 + E^2)D^2$$

$$D = 2S/D_1$$

$$E = D_2/(2S)$$

$$F_{21} = \frac{A_1}{A_2} F_{12} \quad \text{(Reciprocity Law for view factors)} \tag{3.6}$$

$$F_{2L} = 1 - F_{21} \quad \text{(Summation Law for view factors)} \tag{3.7}$$

Note that the view factors are explicit functions of the ratios S/D_1 and D_2/D_1.

Equations 3.2 and 3.4 may be normalized by defining constants k_{12}, K_{1x}, and k_{2x} as follows:

$$\left.\begin{aligned} A_2 &= k_{12}A_1 \\ A_{1x} &= k_{1x}A_1 \\ A_{2x} &= k_{2x}A_2 = k_{2x}k_{12}A_1 \end{aligned}\right\} \tag{3.8}$$

Also, the Reciprocity Law for view factors allows the following substitution to be made:

$$A_2F_{2L} = A_LF_{L2} \tag{3.9}$$

Substituting equations 3.8 and 3.9 into equations 3.2 and 3.4 and dividing by A_1, the only term involving area becomes the term P/A_1 in equation 3.2. All other terms contain only

the "k" constants which are dependent on relative dimensions. The significance of this normalization is that the dual surface configuration may be scaled to any power level by increasing its size. Since the scaling term is an area, linear dimensions of a particular design increase as the square root of the ratio of power levels. For example, increasing the power level from 6.5 to 650 watts would require scaling the linear dimensions of the design by a factor of 10.

The resultant normalized equations become:

$$\sigma\varepsilon_1 T_1^4 = G\alpha_{s1}\sin(\theta)k_{1x} + P/A_1 + \sigma\varepsilon_2 k_{12}F_{21}T_2^4\varepsilon_1 \qquad (3.10)$$

$$\sigma\varepsilon_2 2k_{12}T_2^4 = G\alpha_{s2}\sin(\theta)k_{12} + G(1 - \alpha_{s2})\sin(\theta)k_{1x} +$$

$$G(1-\alpha_L)\sin(\theta)k_{12}k_{2x} + \sigma\varepsilon_L k_{12}F_{2L}T_L^4\varepsilon_2 + \sigma\varepsilon_1 F_{12}T_1^4\varepsilon_2 \qquad (3.11)$$

Equations 3.10 and 3.11 may be solved explicitly for the equilibrium temperature of the primary surface.

$$T_1 = \left[\left[\frac{2}{\sigma\varepsilon_1(2 - F_{21}\varepsilon_1\sigma F_{12}\varepsilon_2)}\right]\left[G\alpha_{s1}\sin(\theta)k_{1x} + P/A_1 + \frac{F_{12}\,\varepsilon_1}{2}\left[G\alpha_{s2}\sin(\theta)k_{12} + G(1 - \alpha_{s2})\sin(\theta)k_{1x} + G(1-\alpha_L)\sin(\theta)k_{12}k_{2x} + \sigma\varepsilon_L k_{12}F_{2L}T_L^4\varepsilon_2\right]\right]\right]^{1/4} \qquad (3.12)$$

Since the view factors are explicit functions of S/D_1 and D_2/D_1, the temperature of the primary surface may be written as

$$T_1 = T_1(P/A_1,\ S/D_1,\ D_2/D_1,\ \ ,z_1,\ z_2,\ \ldots\ z_n) \tag{3.13}$$

where $z_1,\ z_2,\ \ldots\ z_n$ are constants containing G, α_s, ε, etc.

Equation 3.13 is used as the basis for subsequent discussion of optimization parameters for the dual surface configuration.

3.3.3 Typical Dual Surface Configuration

Before proceeding with the optimization of the dual surface design, it is worthwhile to present a simple example demonstrating the thermal performance characteristics of a typical configuration. The configuration for example #1, shown in Figure 3.9 , represents an initial estimate of possible design parameters for the SEP receiver. The parameter $P/A = 13$ watts/ft^2 represents acompromise between allowable physical size of the experiment package and required area to dissipate internal power. The separation parameter S/D_1 is large enough to reduce secondary IR absorbed by the primary surface, but small enough to shade the primary at high solar elevations which result in excessive temperatures for unshaded surfaces. The parameter D_2/D_1 is set equal to unity for the first example.

The temperature of the primary surface for example #1 is plotted as a function of solar elevation and surface degradation in Figure 3.10.

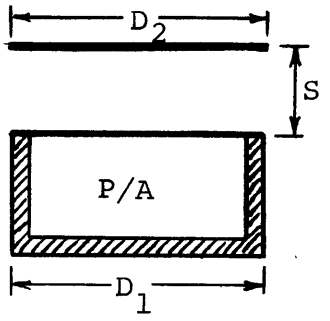

$P/A = 13$ watt/ft^2

$S/D_1 = .40$

$D_2/D_1 = 1.0$

Figure 3.9 - Basic Dual Surface Configuration, Example #1

3.3.4 Observations

Several important observations may be made from Figure 3.10.

1) The minimum temperature for the dual surface design is higher than for the single surface design (Figure 2.2A), but still falls below the minimum allowable temperature for the SEP experiment (5°C).

2) The maximum temperature for the dual surface design of example #1 does not occur at $\theta = 90°$. Instead, the temperature of the primary surface actually decreases at high sun elevations because the secondary surface is providing more

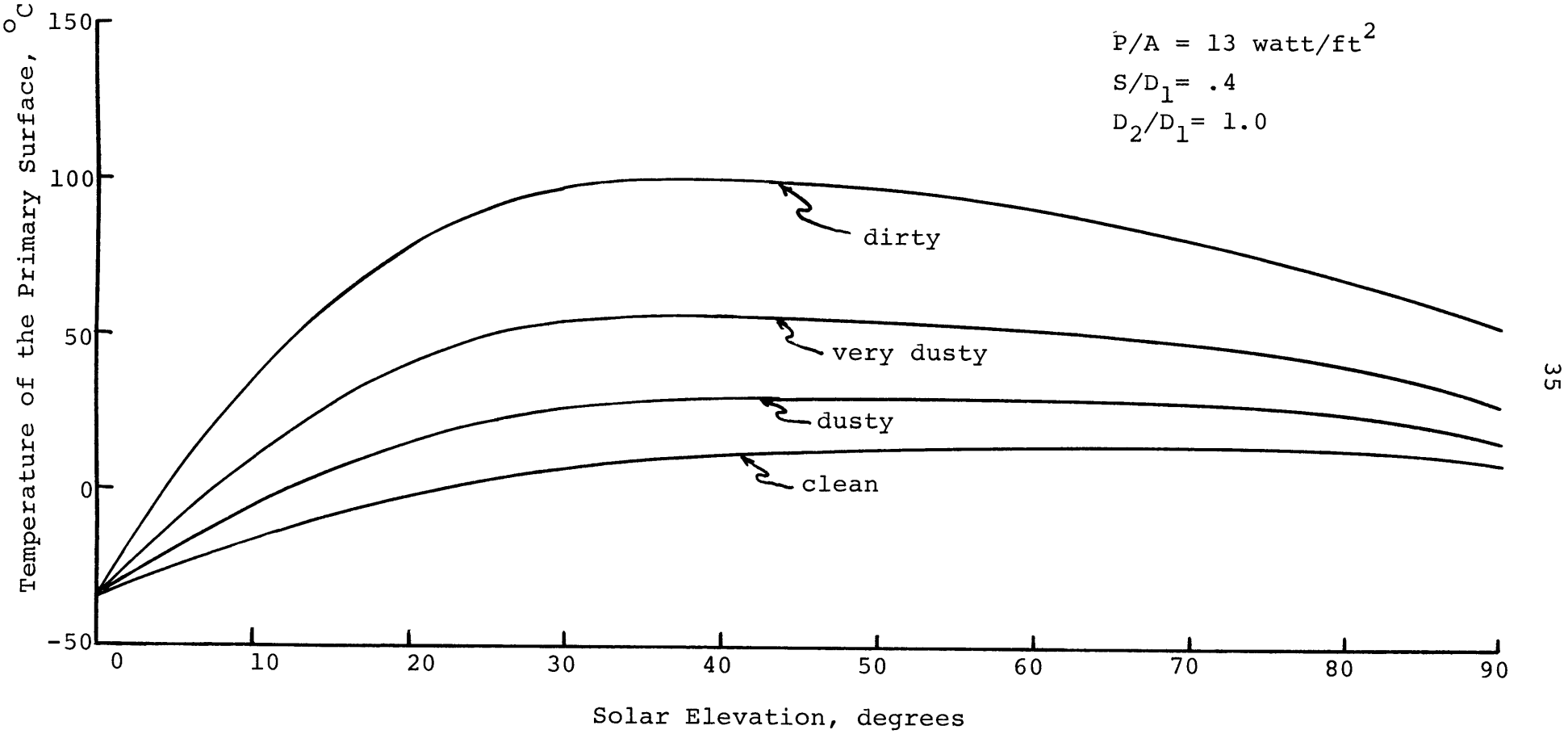

Figure 3.10 - Thermal Performance of Basic Dual Surface Configuration, Example #1

shade. The decrease in primary surface temperature at high solar elevations is limited by the fact that the secondary is absorbing more energy from the lunar surface and the sun. Some of this absorbed energy is reradiated to the primary surface, partially compensating for the shading provided by the secondary.

3) The primary surface temperature shows less sensitivity to dust degradation than for the single surface design. The single surface design, with P/A = 13 wt/ft^2, fluctuates over a range of 143°C at $\theta = 90°$ due to dust degradation of the radiative surface. The primary surface in a dual surface design under identical circumstances varies only 55°C.

4) The maximum temperature of the primary surface in a dual surface design is lower than the maximum temperature for a single surface design. In fact, the maximum temperature for example #1 under very dusty conditions exceeds the maximum allowable temperature for the SEP receiver (50°C) by only 6°C.

3.3.5 P/A Parameter for the Dual Surface Concept

An extremely important parameter for radiative surface thermal protection systems is the value of the ratio P/A.

Equation 3.12 may be reduced to an equation of the form

$$T_1 = \sqrt[4]{C_1 + C_2(P/A_1)} \qquad (3.14)$$

where C_1 and C_2 are functions of constants other than P/A_1, and $C_2 < C_1$ for cases of relevance to the SEP experiment.

Therefore, for a given power level, increasing the area decreases temperatures at all sun elevations. As the area becomes very large, the increase in area has less and less effect and the thermal performance approaches that of a configuration with no internal power dissipation.

Example #2 demonstrates quantitatively the effect of changing the value of P/A by decreasing the value of P/A in example #1 to 6.5 watt/ft^2. The temperature of the primary surface for example #2 is plotted in Figure 3.11 as a function of solar elevation and surface degradation.

Note that the minimum primary surface temperatures are decreased more than the maximum temperatures. If the parameter P/A is used to decrease maximum temperatures, two consequences must be considered: 1) the physical size of the configuration must be increased, and 2) it becomes more difficult to maintain minimum operating temperatures at low solar elevations.

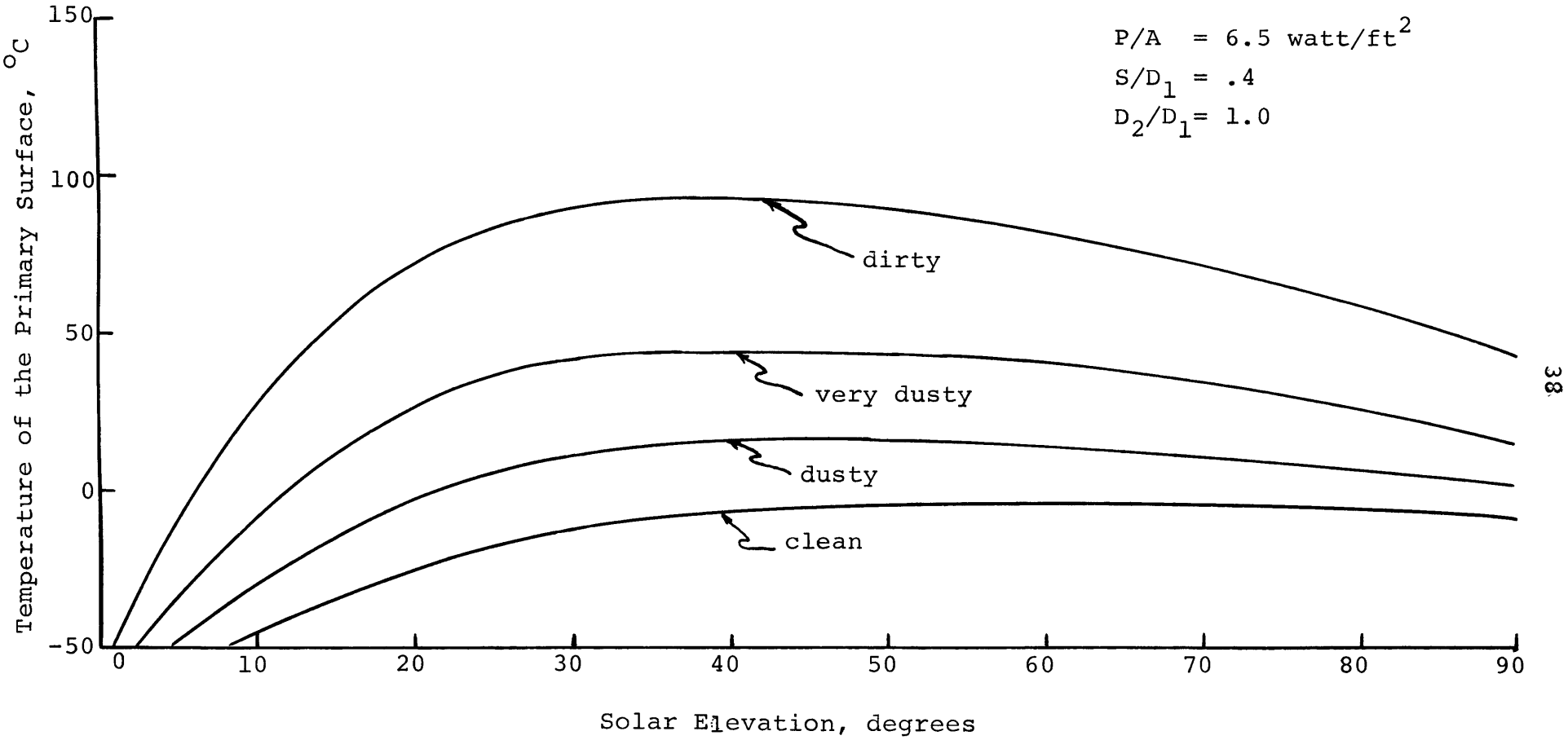

Figure 3.11 - Thermal Performance of Basic Dual Surface Configuration With Modified Ratio of P/A, Example #2

3.3.6 Optimization of S/D_1 and D_2/D_1 Parameters

The performance of the configurations for examples #1 and #2 may be improved by seeking optimum values for the parameters D_2/D_1 and S/D_1. Figure 3.12 shows the relation of the minimum and maximum temperatures of the primary surface to the variable S/D_1. This figure is generated by iterating the parameter S/D_1 in equation 3.12 for all solar elevations and noting the minimum and maximum temperature for each iteration of the separation parameter. From Figure 3.12 it is seen that the value $S/D_1 = .25$ yields the lowest maximum temperatures and highest minimum temperatures for $P/A = 13$ watt/ft^2 and $D_2/D_1 = 1.0$. It is important to remember that changing the parameter S/D_1 changes not only the maximum temperature incurred by the primary surface, but also the solar elevation at which the maximum temperature will occur.

Figure 3.13 is generated in a manner similar to Figure 3.12 and shows the relation of minimum and maximum primary surface temperatures to the variable D_2/D_1 with $P/A = 13$ watt/ft^2 and $S/D_1 = .25$. The parameter D_2/D_1 is not nearly as significant as the parameters P/A and S/D_1, as seen from the very flat curves of Figure 3.13. From Figure 3.13, it is seen that a value of $D_2/D_1 = 1.1$ slightly improves the thermal performance of example #1 by lowering the maximum temperature by one or two degrees centigrade.

Physically, the parameters S/D_1 and D_2/D_1 are effecting the tradeoff between solar energy and reradiated IR energy.

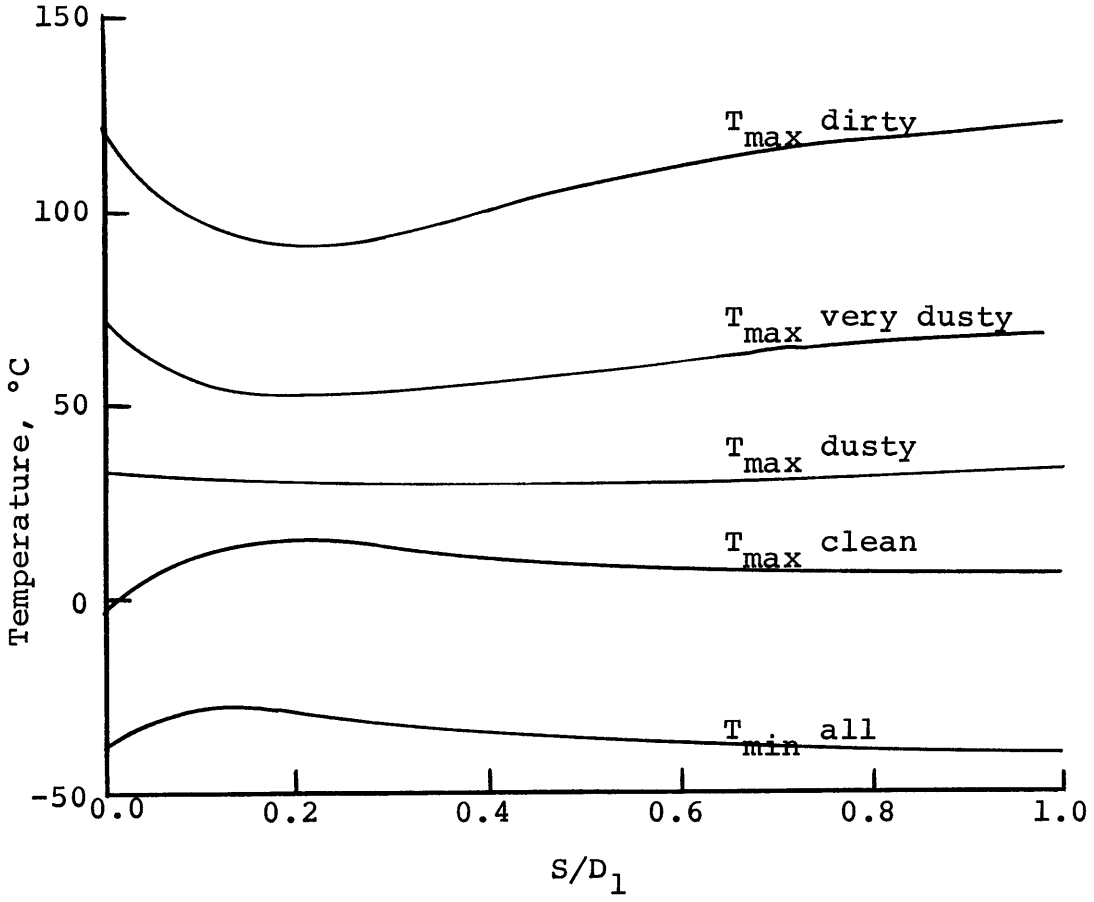

Figure 3.12 - Optimization of S/D_1 Parameter

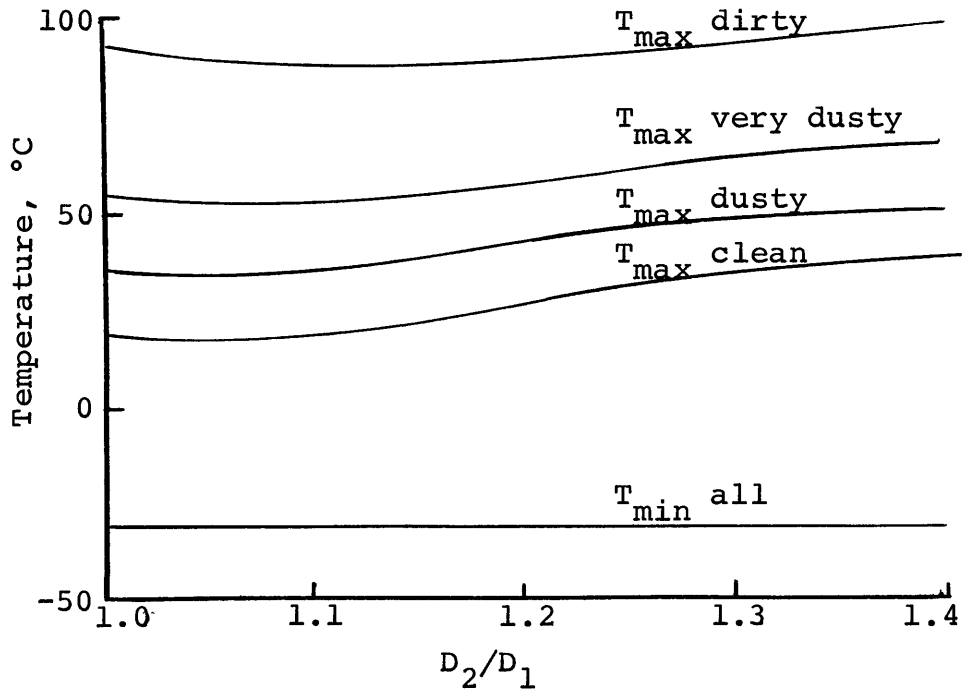

Figure 3.13 - Optimization of D_2/D_1 Parameter

As the separation of the surfaces in a dual surface design is decreased, two effects tend to lower the temperature of the primary surface: i) the primary is more shaded from solar flux, and ii) the secondary absorbs less lunar IR. At the same time, however, the view factors F_{12} and F_{21} increase tending to raise the temperature of the primary surface. Conversely, if the separation is increased, the view factors are decreased and the primary surface is exposed to more solar energy. Increasing D_2/D_1 causes the primary surface to be shaded more quickly as the solar elevation changes, as shown in Appendix A, but it also allows the secondary to absorb more energy in the form of lunar IR and solar flux.

Figure 3.14 describes the configuration for example #3. This is a near optimum planar dual surface design generated using Figures 3.12 and 3.13. The thermal performance of example #3 is plotted in Figure 3.15. The effects of optimization may be seen by comparing the thermal performance of example #1 and example #3 (Figures 3.10 and 3.15). The maximum temperatures have been lowered, and the temperatures at very high sun elevations have been raised slightly. The result is a flattening of the thermal performance curve with a resultant lower maximum temperature and higher minimum temperature.

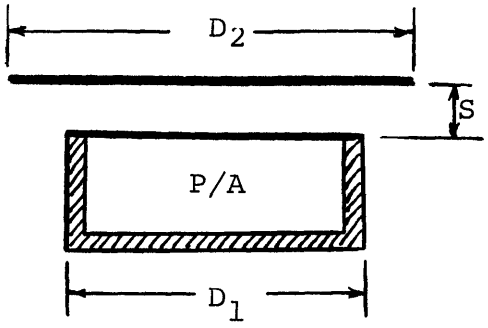

$P/A = 13 \text{ watt/ft}^2$

$S/D_1 = .25$

$D_2/D_1 = 1.1$

Figure 3.14 - Dual Surface Configuration with Optimum Values of S/D_1 and D_2/D_1

The maximum temperature for very dusty conditions is 53°C, only 3° above the allowable maximum for SEP operation. The minimum temperature is -31°C which is much too low for SEP, but it should be noted that this temperature rises quickly to 6°C at 25° solar elevation under clean conditions. Thus, for applications not requiring operational temperatures at low solar elevations, such a design may be acceptable. Chapter five discusses several methods of raising minimum temperatures at low solar elevations.

3.4 Multi-Secondary Configurations

It is readily apparent that the qualitative arguments of section 3.2 may be applied to controlling the temperature of the secondary surface. It has been shown that the dual surface design helps heat the lower surface at low solar elevations and helps cool it under dirty conditions at high solar elevations. There is no reason that a that a third,

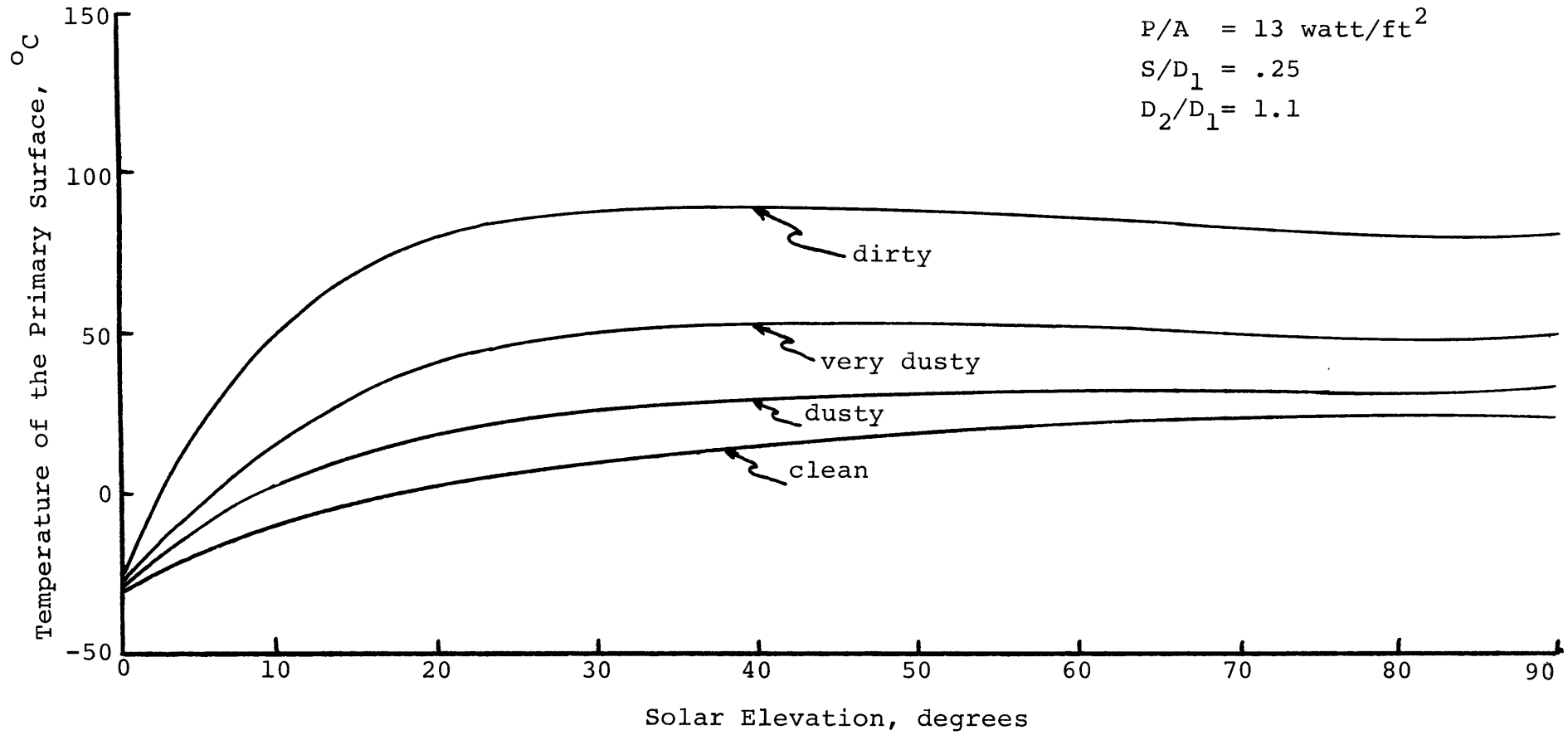

Figure 3.15 - Thermal Performance of Optimum Dual Surface Configuration, Example #3

fourth, or fifth parallel plate could not be added, each heating or cooling the surface below it. Such a configuration is shown in Figure 3.17.

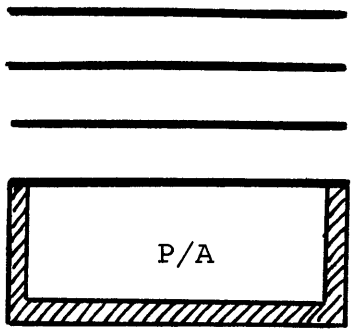

Figure 3.16 - Multi-Secondary Configuration

Since a systematic computer iteration of key parameters for multi-secondary configurations showed only marginal potential for improvement of primary surface thermal performance, the discussion of equilibrium equations and optimization parameters will be omitted. These follow the same basic form as for simple dual surface designs.

The configuration of example #4 is shown in Figure 3.17. It is identical to example #1 except that an additional flat plate has been added above the original secondary. The thermal performance of example #4 is shown in Figure 3.18. Relative to example #1, the multi-secondary configuration has a slightly higher (approximately 3°C) minimum temperature, a slightly higher maximum temperature, and a much lower

(approximately 30°C) temperature of the primary surface at high sun elevations. The effect of the extra surface is to accentuate the "hump" in the thermal performance curve of example #1.

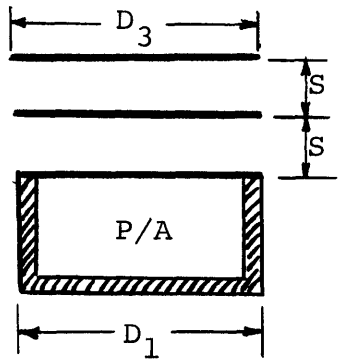

$P/A = 13$ watt/ft^2

$D_3 = D_2 = D_1$

$S/D_1 = .4$

Figure 3.17 - Multi-Secondary Configuration, Example #4

Example #4 is not an optimum design for a multi-secondary configuration. Numerical results indicate that an optimum design is capable of slightly improving thermal performance at all solar elevations, although the reduction in maximum temperature of the primary surface is only a few degrees centigrade for a value of $P/A = 13$ watt/ft^2.

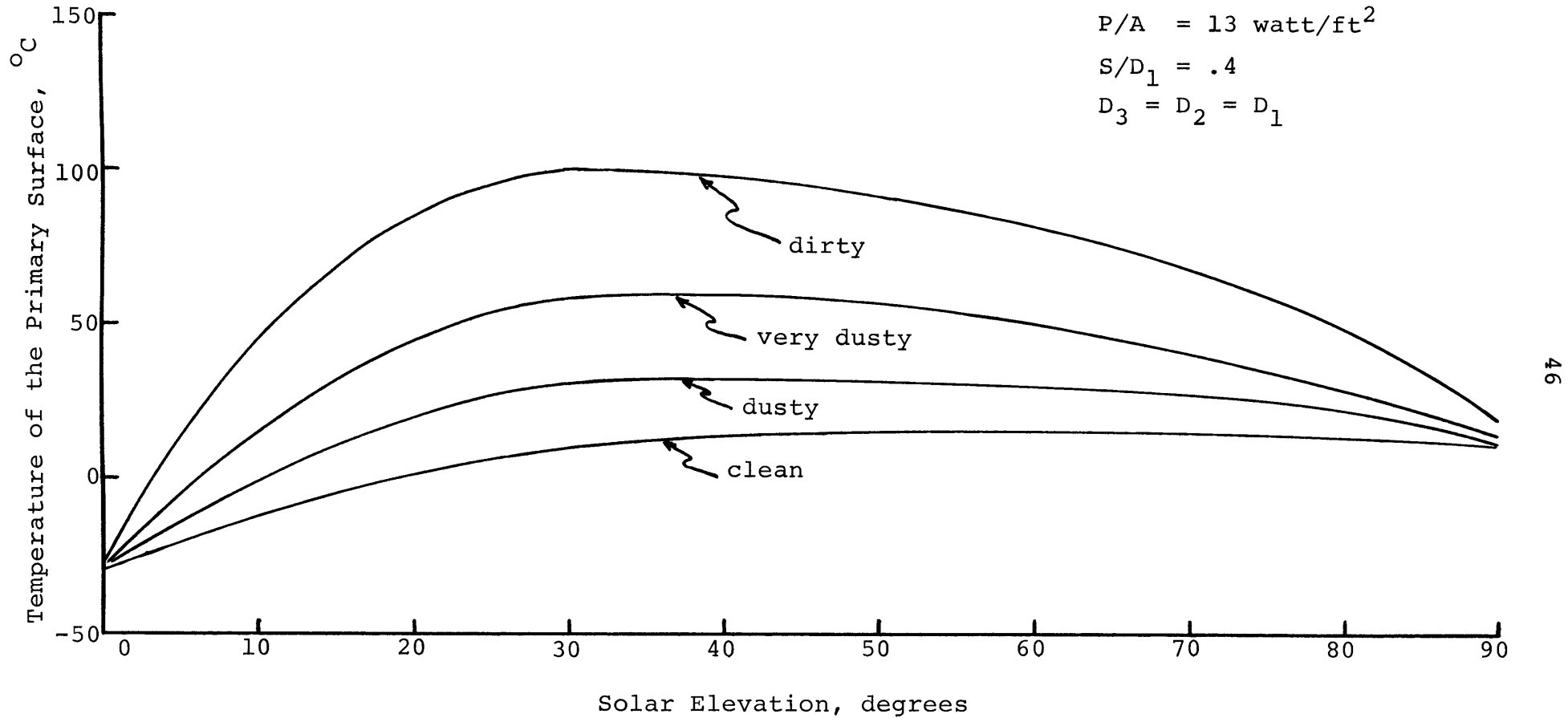

Figure 3.18 - Thermal Performance of Multi-Secondary Dual Surface Configuration, Example #4

CHAPTER 4

CONICAL SECONDARY SURFACES

4.1 Introduction

The basic dual surface model with planar surfaces can be improved in two ways: 1) by raising the minimum temperature of the primary surface at low solar elevations, and 2) by lowering the maximum temperature of the primary surface, which occurs at approximately 30 to 45 degrees solar elevation. It will be shown in this chapter that conical secondary surfaces achieve both of the objectives.

Consider the dual surface configuration shown in Figure 4.1. At low solar elevations, one side of the cone absorbs solar energy, whereas a flat plate secondary design absorbs none. It will be quantitatively demonstrated later on that this results in a higher minimum temperature for the primary surface at low solar elevations. At high solar elevations, the effective absorbing area of the cone is the same as that for a flat plate. This is illustrated in Figure 4.2. However, the radiative area of the conical surface is much greater than the surface area of a flat plate, and in addition the conical surface absorbs lunar IR. It will be shown both analytically and quantitatively that at high solar elevations the increase in radiative area is more significant than the increase in absorption of lunar IR. This results in a lower maximum temperature of the primary surface.

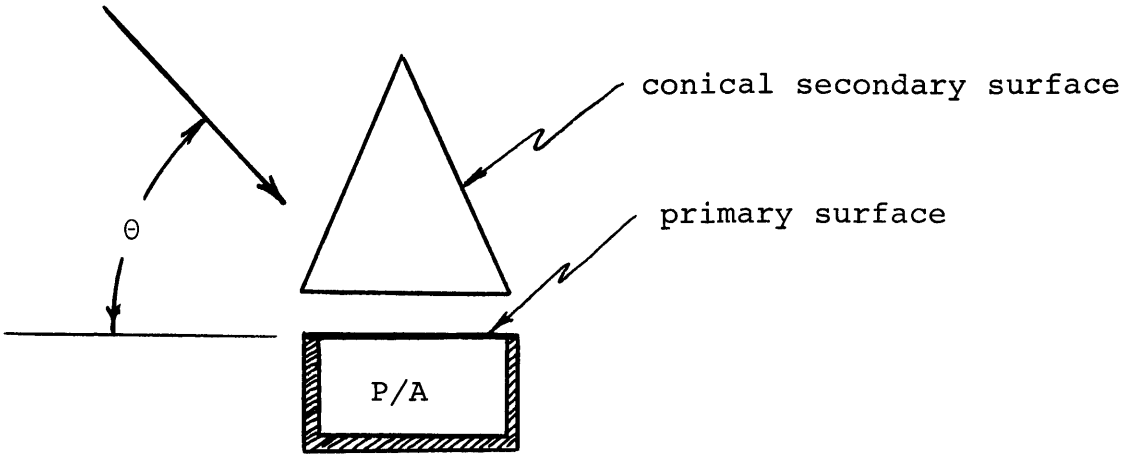

Figure 4.1 - Dual Surface Model With Conical Secondary Surface

side view (Θ = 0)

perspective view (low Θ)

perspective view (high Θ)

effective absorbing area (high Θ)

Figure 4.2 - Effective Absorbing Area of a Cone at High Solar Elevations

4.2 Analytic Development, High Solar Elevations

The following brief analytic development serves two purposes: 1) it demonstrates the physical mechanism by which conical secondaries improve flat plate secondary thermal performance, and 2) it provides a necessary check on the consistency of the computer results described in section 4.4.

Conical and flat plate secondaries may be compared at a given solar elevation by considering only the energy transfers taking place on the upper secondary surface. The distinction between "upper" and "lower" secondary surfaces, in this context, is made clear in Figure 4.3.

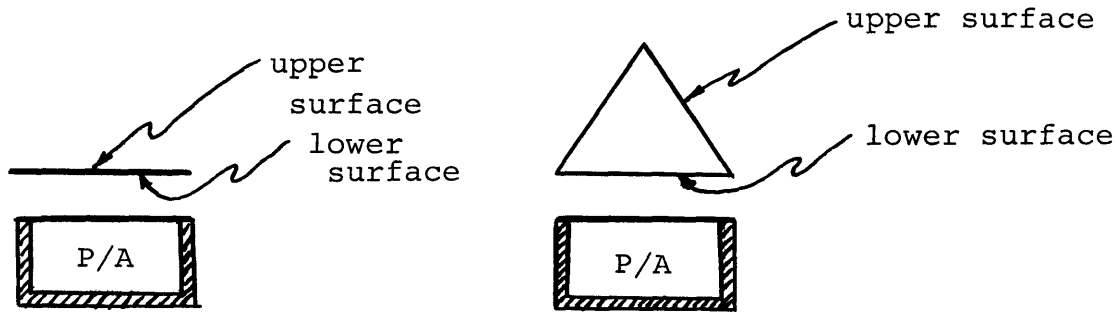

Figure 4.3 - Upper and Lower Secondary Surface

Figure 4.4 shows a conical secondary, insulated on the bottom so that energy transfers of only the upper surface are considered. For $\beta = 180°$ this secondary becomes a flat plate, and for $\beta = 90°$ it becomes an infinite cylinder. The thermal equilibrium equation for this conical surface allows direct comparison of flat plates, cones, and cylinders

as a means of controlling secondary surface temperatures at a given solar elevation.

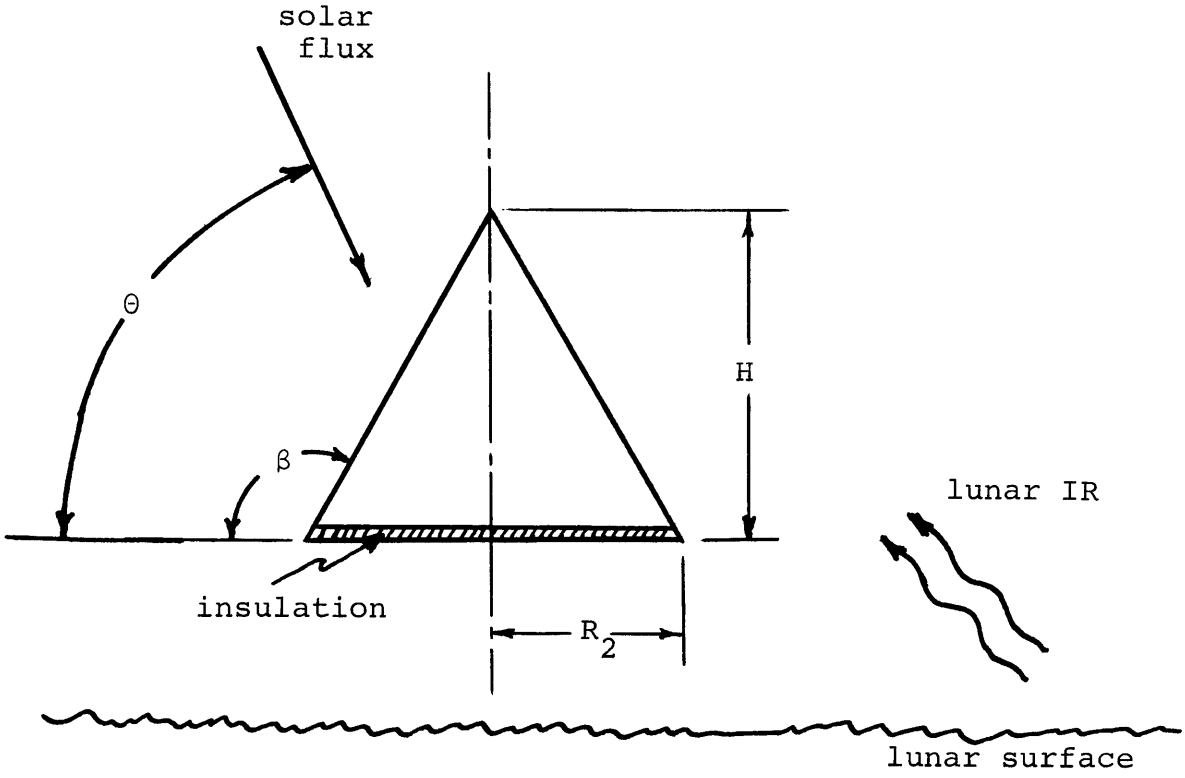

Figure 4.4 - Conical Secondary Surface
Neglecting Bottom Interactions

The thermal equilibrium equation for Figure 4.4 is

$$\begin{bmatrix}\text{energy}\\ \text{radiated}\end{bmatrix} = \begin{bmatrix}\text{solar energy}\\ \text{absorbed}\end{bmatrix} + \begin{bmatrix}\text{lunar IR}\\ \text{absorbed}\end{bmatrix}$$

$$\sigma\varepsilon_2 T_2^4 A_{2T} = G\alpha_2 A_{eff} + \sigma\varepsilon_L T_L^4 A_{2T} F_{2TL} \varepsilon_2 \qquad (4.1)$$

where F_{2TL} = the geometric view factor representing the fraction of energy emitted by the upper conical surface that is incident on the lunar surface. Note that equation 4.1 uses the identity $A_L F_{L2T} = A_{2T} F_{2TL}$ (Reference 4).

$$F_{2TL} = 1/2\ (1 + \cos\ \beta) = 1/2\ (1 - \frac{R_2}{\sqrt{R_2^2 + H^2}})$$

A_{2T} = total conical surface area

$$= \pi R_2 \sqrt{R_2^2 + H^2}$$

A_{eff} = effective absorbing area of a cone

$$= \pi R_2^2 \sin(\theta) \text{ for } \pi - \beta \leq \theta \leq \beta \text{ and } \beta \geq \frac{\pi}{2}$$

$$\sigma \varepsilon_2 T_2^4 \pi R_2 \sqrt{R_2^2 + H^2} = G\alpha_2 \pi R_2^2 \sin(\theta) + G\alpha_L \sin(\theta) \pi R_2 \sqrt{R_2^2 + H^2}\ \ 1/2\ (1 - \frac{R_2}{\sqrt{R_2^2 + H^2}})\ \varepsilon_2$$

$$T_2^4 = \frac{G\pi R_2 \sin(\theta)}{\sigma \varepsilon_2 \pi R_2} \left[\frac{R_2 \alpha_2 + \alpha_L \sqrt{R_2^2 + H^2}\ 1/2\ \varepsilon_2 - \alpha_L \frac{1}{2} R_2 \varepsilon_2}{\sqrt{R_2^2 + H^2}} \right]$$

$$T_2 = T_L\left[\frac{R_2}{\sqrt{R_2^2 + H^2}}\,(\alpha_2 - 1/2\,\varepsilon_2) + 1/2\,\varepsilon_2\right]^{1/4} \qquad (4.2)$$

where $\alpha_L = 1.0$

$\varepsilon_2 = \varepsilon_L = .85$

and $T_L \equiv \sqrt{\dfrac{G\alpha_L \sin(\Theta)}{\sigma\varepsilon L}}$

From equation 4.2 it is seen that as the value of H becomes very large, the quantity $\dfrac{R_2}{\sqrt{R_2^2 + H^2}}\,(\alpha_2 - 1/2\,\varepsilon_2)$ approaches zero. This quantity may approach zero from the positive or negative side depending on the values of α_2 and ε_2. For highly degraded surfaces, $\alpha_2 > 1/2\,\varepsilon_2$ and the expression is always positive. Under these circumstances, T_2 is a minimum for large values of H. Conversely, for clean surfaces ($\alpha_2 < 1/2\,\varepsilon_2$) T_2 is a minimum for $H = 0$.

The physical mechanism that allows T_2 to be minimized is the radiative surface area, which contributes the term $\sqrt{R_2^2 + H^2}$ to the denominator of equation 4.2. For $\pi-\beta \leq \Theta \leq \beta$ the conical secondary absorbs the same amount of solar energy as a flat plate, but has a larger radiative surface area. The conical secondary also absorbs more lunar IR, but the increased absorption is not as significant as the increase in radiative power.

Equation 4.2 may not be used to compare the overall thermal performance of conical secondaries, since the restriction $\theta > \pi - \beta$ omits low solar elevations from consideration. For cones with large values of H, the omitted values of solar elevation become quite important since the omitted elevations include those at which the maximum temperatures of the primary surface occur. A rigorous analysis, valid at all solar elevations, requires the use of a general treatment for the effective absorbing area of a conical surface (A_{eff}), which is given in Appendix B. The comparison of conical secondaries, using a general formulation for A_{eff}, is much more complex than the preceeding analysis which has been restricted to $\pi - \beta \leq \theta \leq \beta$. For this reason the general analysis will be carried out numerically on a computer. The necessary equilibrium equations for the general comparison are given in section 4.3, and the conclusions based on the computer results are presented in section 4.4.

4.3 Generalized Thermal Equilibrium Equations

The thermal equilibrium equations for the dual surface configuration of Figure 4.1 may be written as follows.

Equilibrium of the primary surface:

$$\begin{bmatrix}\text{Energy}\\ \text{radiated}\end{bmatrix} = \begin{bmatrix}\text{solar energy}\\ \text{absorbed}\end{bmatrix} + \begin{bmatrix}\text{internal}\\ \text{dissipation}\end{bmatrix} + \begin{bmatrix}\text{secondary IR}\\ \text{absorbed}\end{bmatrix} \tag{4.3}$$

Equilibrium of the secondary surface:

$$\begin{bmatrix}\text{Energy radiated}\\ \text{(all surfaces)}\end{bmatrix} = \begin{bmatrix}\text{direct solar}\\ \text{energy absorbed}\end{bmatrix} + \begin{bmatrix}\text{solar energy}\\ \text{reflected from}\\ \text{primary surface}\end{bmatrix}$$

$$+ \begin{bmatrix}\text{lunar albedo}\\ \text{absorbed}\end{bmatrix} + \begin{bmatrix}\text{lunar IR}\\ \text{absorbed}\end{bmatrix} + \begin{bmatrix}\text{IR from primary}\\ \text{surface absorbed}\end{bmatrix} \tag{4.4}$$

The general form of the equilibrium equations for conical secondaries remains the same as for planar secondaries in chapter 3. Only three terms of equation 4.4 require formulation different from the equilibrium equations for planar dual surface configurations, as shown below.

$$\begin{bmatrix}\text{energy radiated}\\ \text{(all surfaces}\end{bmatrix} = \sigma\varepsilon_2(A_{2B} + A_{2T})T_2^4$$

$$\begin{bmatrix}\text{direct solar energy}\\ \text{absorbed}\end{bmatrix} = G\alpha_{s2}A_{eff} \tag{4.5}$$

$$\begin{bmatrix}\text{lunar IR}\\ \text{absorbed}\end{bmatrix} = \sigma\varepsilon_L(A_{2B}F_{2BL} + A_{2T}F_{2TL})T_L^4\varepsilon_2$$

where A_{2B} = area of the bottom of the secondary surface

A_{2T} = area of the upper secondary surface

A_{eff} = effective absorbing area of the secondary

F_{2BL} = geometric view factor of the bottom of the secondary to the lunar surface (Reference 4).

The normalization of these equations follows in the same manner as for planar dual surface configurations by defining

$$A_{2B} = k_{12B}A_1$$
$$A_{2T} = k_{12T}A_1 \qquad (4.6)$$
$$A_{eff} = k_{12T}A_1$$

The normalized equilibrium equations for dual surface configurations with conical secondaries follow from equations 3.10, 3.11, 4.5 and 4.6.

Equilibrium of the primary surface:

$$\sigma\varepsilon_1 T_1^4 = G\alpha_{s1}k_{1x}\sin(\theta) + \frac{P}{A_1} + \sigma\varepsilon_2 k_{12B}F_{2B1}T_2^4\varepsilon_1 \qquad (4.7)$$

Equilibrium of the secondary surface:

$$\sigma\varepsilon_2(k_{12B} + k_{12T})T_2^4 = G\alpha_{s2}k_{12eff} + G(1 - \alpha_{s1})k_{1x}\sin(\theta)$$
$$+ \sigma\varepsilon_L(k_{12B}F_{2BL} + k_{12T}F_{2TL})T_L^4\varepsilon_2 + \sigma\varepsilon_1 T_1^4 F_{12B}\varepsilon_2 \qquad (4.8)$$

where the albedo term is included in the lunar IR term by setting $\alpha_L = 1.0$.

Equations 4.7 and 4.8 have been used to calculate the thermal performance of conical dual surface configurations in the computer analysis described in the following section.

4.4 Computer Analysis

This section presents the results of a systematic computer study based on equations 4.7 and 4.8 with the objective of identifying the conical secondary that yields the best overall thermal performance of a dual surface configuration. General observations concerning conical secondaries are made and a specific example is discussed, but detailed presentation of numerical results is considered beyond the scope of this thesis.

4.4.1 Cylindrical Secondaries

Numerical comparison of cylindrical secondaries relative to flat plate and conical secondaries results in the conclusions of Table 4.1 below.

TABLE 4.1 - COMPARATIVE THERMAL PERFORMANCE OF CYLINDRICAL SECONDARIES TO FLAT PLATE AND CONICAL SECONDARIES

Solar elevation	Temperature of the primary surface using cylindrical secondary (relative to flat plate or conical secondaries)	
	clean	dirty
0°	no change	raises
elevation at which maximum temperatures occur	raises	raises
90°	raises	lowers

Three significant observations may be made concerning cylindrical secondaries: 1) The results of Table 4.1 are consistent with previous conclusions drawn from equation 4.2; 2) Since the maximum temperature is increased slightly, and the minimum temperature is relatively uneffected under clean conditions, the cylindrical secondary is not the best choice for satisfying SEP thermal requirements; 3) The increase in temperature at $\Theta = 45°$ could not have been predicted from equation 4.2 since the requirement $\Theta \geq \pi - \beta$ is not satisfied.

4.4.2 Conical Secondaries

Conical secondaries have the same qualitative effects in thermal performance as cylindrical secondaries (see Table 4.1), except for maximum temperatures under degraded conditions, which are lowered for certain conical secondaries.

The maximum temperature of the primary surface, under degraded conditions, is slightly less than for flat plate and cylindrical secondaries, but only for a small range of the angle β (approximately 110° to 130°). This range represents the best tradeoff of solar and lunar IR absorption at the solar elevation for which maximum temperatures of the primary surface occur. The optimum value of β changes slightly with surface conditions, but not enough to become a practical consideration.

The computer results for conical secondaries are again consistent with equation 4.2 in several ways. First, for

$\beta = 180°$, the results agree with previous results for flat plate designs. Second, increasing the value of H always decreases temperatures of the primary surface under degraded conditions for $\pi - \beta \leq \Theta \leq \beta$ and $\frac{\pi}{2} \leq \beta \leq \pi$.

4.4.3 Optimum Conical Secondary

Example #5 (Figure 4.5) represents a conical dual surface configuration with the best values of the separation parameter (S/D_1) and the conical angle (β), as determined from numerical computer results for several iterations of S/D_1 and β using equations 4.7 and 4.8. The parameter D_2/D_1 is set equal to one and not iterated since it has been shown in chapter 3 to have little effect on dual surface optimization. The parameter P/A is set at the value of 13 watt/ft^2 for purposes of comparison with previous examples. Figure 4.6 shows the thermal performance of the example #5.

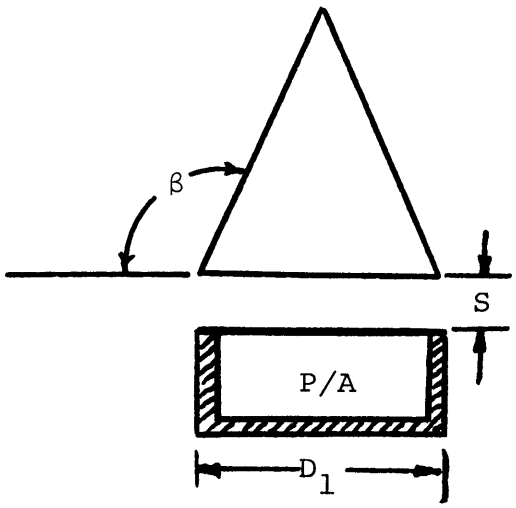

$P/A = 13$ watt/ft^2

$\beta = 120°$

$S/D_1 = .25$

$D_2/D_1 = 1.0$

Figure 4.5 - Optimum Dual Surface Configureation with Conical Secondary, Example #5

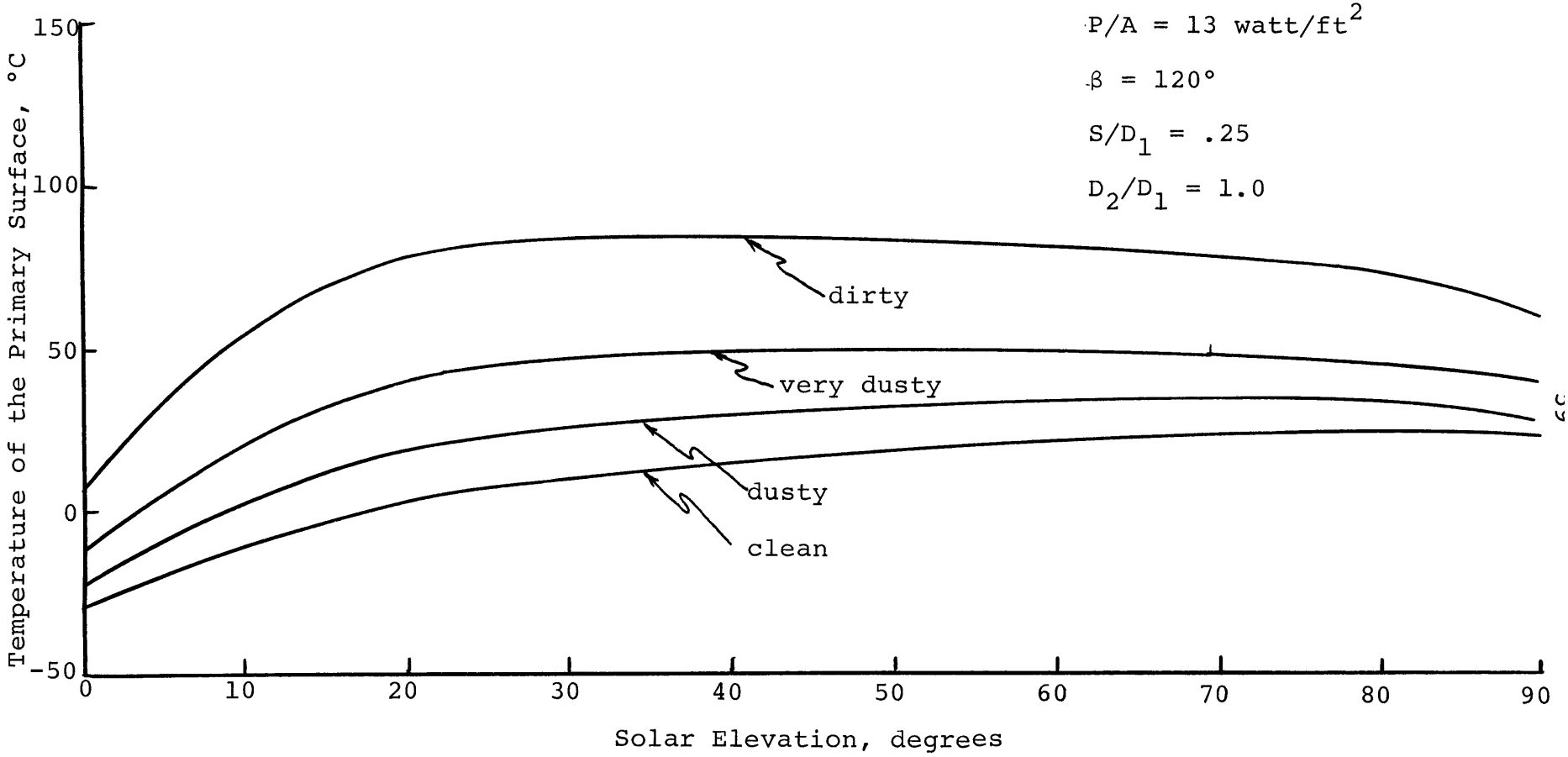

Figure 4.6 - Thermal Performance of Dual Surface Configuration With Optimum Conical Secondary, Example #5

The thermal performance of this configuration is acceptable, except at low solar elevations. For clean, dusty, and very dusty conditions the maximum temperature is less than 50°C. At solar elevations less than 30°, the minimum temperature of the primary surface is below 5°C and must be raised to satisfy SEP thermal requirements.

CHAPTER 5

EXTENSIONS

This chapter briefly describes several methods of further improving the thermal performance of simple dual surface configurations (see Table 5.1). It is intended as a foundation for future work, and as such, attempts to convey concepts, not quantitative results. It is felt that these ideas offer very good potential for designing light-weight thermal protection systems for dusty and mobile lunar environments.

TABLE 5.1 - THERMAL PERFORMANCE OF EXAMPLE CONFIGURATIONS

Example	Configuration	Parameters			Minimum Temperature ^{o}C, Clean	Maximum Temperature (^{o}C)	
		P/A (wt/ft^2)	S/D_1	D_2/D_1		very dusty	dirty
-	Simple radiative surface	13	-	-	-41	74	140
		6.5	-	-	-78	65	134
#1	Typical Dual Surface	13	.4	1.0	-35	56	100
#2	Typical Dual Surface, low P/A ratio	6.5	.4	1.0	-72	45	92
#3	Optimum Dual Surface	13	.25	1.1	-31	53	89
#4	Multi-secondary	13	.4	1.0	-33	58	101
#5	Optimum conical secondary ($\beta=120^{o}$)	13	.25	1.0	-29	50	83
#6	Optimum conical secondary with solar powered heater ($\beta=120^{o}$, $H_p = D_1$)	13	.25	1.0	8	50	83

5.1 Solar Powered Heater

One method of raising the minimum temperature of any configuration is to use solar cells to power an internal heater. This method is preferred over alternatives such as thermal switches because an electronic thermostat is inherently more reliable than a mechanical thermal switch. However, the major disadvantages of such a system are the larger size and weight requirements for the solar panel due to axially symmetric constraints for mobile experiments, and the relatively low (10%) efficiency of energy conversion.

An example (Figure 5.1) has been studied to determine the feasibility of this type system. The following points were examined: (a) the degradation of solar cell performance under high temperatures (b) the degradation of solar cell performance under dusty conditions, and (c) solar panel size required for achieving the minimum allowable temperature at low solar elevations.

The following assumptions have been made for this example:

1) Change in nominal solar cell efficiency (10%) due to degrading surface conditions is linear. This results in 10% efficiency under clean conditions and 0% efficiency under dirty conditions.
2) Degradation of solar efficiency due to high temperatures is -.54% per degree centigrade above

27.8°C. Temperature of the solar array is determined on the basis of α_s = .85, ε = .85 under all surface conditions.

3) The heater is controlled by an electronic thermostat set at 25°C. This temperature is arbitrary and is restricted only by the thermal requirements of the experiment.

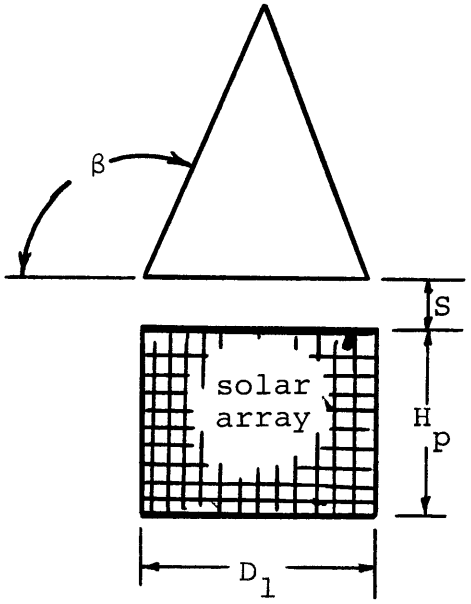

P/A = 13 watt/ft^2
β = 120°
S/D_1 = .25
D_2/D_1 = 1.0
$H_p = D_1$

Figure 5.1 - Dual Surface Design With Solar Powered Heater, Example #6

Example #6 is dimensioned as in Figure 5.1. In general, the solar array may be as large or small as necessary. The purpose of this example is to demonstrate the performance of a typical configuration relating to SEP receiver requirements. This configuration is identical to example #5 except for the addition of the solar powered heater. The thermal

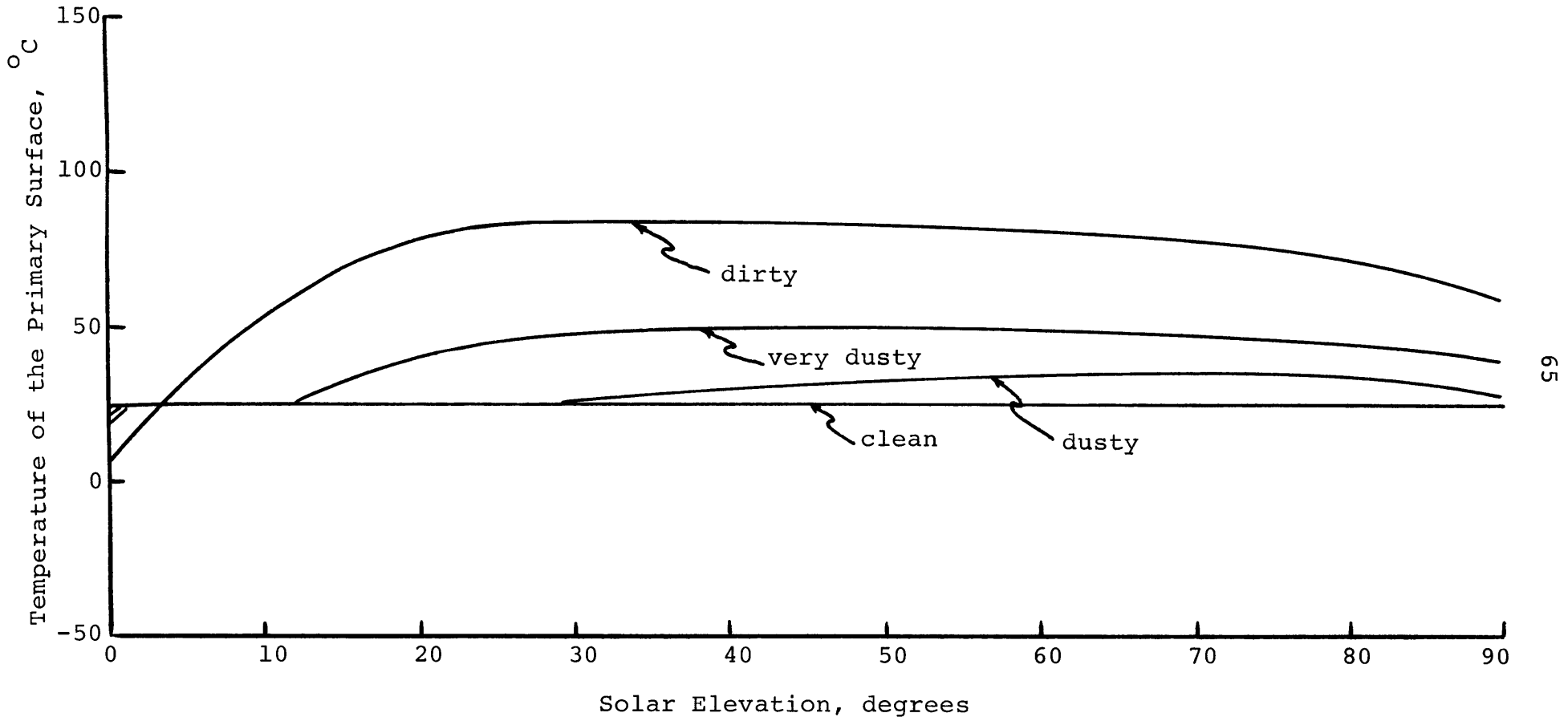

Figure 5.2 - Thermal Performance of Conical Dual Surface Configuration With Solar Powered Heater, Example #6

performance of example #6 is shown in Figure 5.2. For clean conditions, the heater results in a flat curve at 25°C. For dusty, very dusty, and dirty conditions, the minimum temperature is less than 25°C at low solar elevations. Under these conditions the efficiency of the solar array is degraded and cannot heat the internal electronics to 25°C. For dirty conditions, the solar array is completely ineffective as a source of electrical power, but the conical secondary absorbs enough solar energy to maintain minimum SEP thermal requirements (5°). The heater has no effect on temperatures above 25°C since the thermostat turns the heater off. This configuration satisfies thermal requirements for the SEP receiver under clean, dusty, and very dusty conditions, but exceeds the maximum allowable temperature (50°C) for dirty conditions.

5.2 Variable Area Systems

Variable area systems are another means of controlling the temperature of the primary surface. By reducing the area of the primary surface at low solar elevations, the value of the ratio P/A is increased. As seen from equation 3.14, the temperature may be increased to very high levels by allowing the area to approach zero.

Several methods exist for varying the area of the primary surface. One method is the use of a simple bimetallic activator as shown in Figure 5.3. When the configuration is cold, the spring rotates the exposed radiative area underneath an insulating surface, and

replaces it with a non-radiative surface. As the temperature rises, the exposed radiative area is increased. Such a system is simple, lightweight, and has been used frequently in previous space applications.

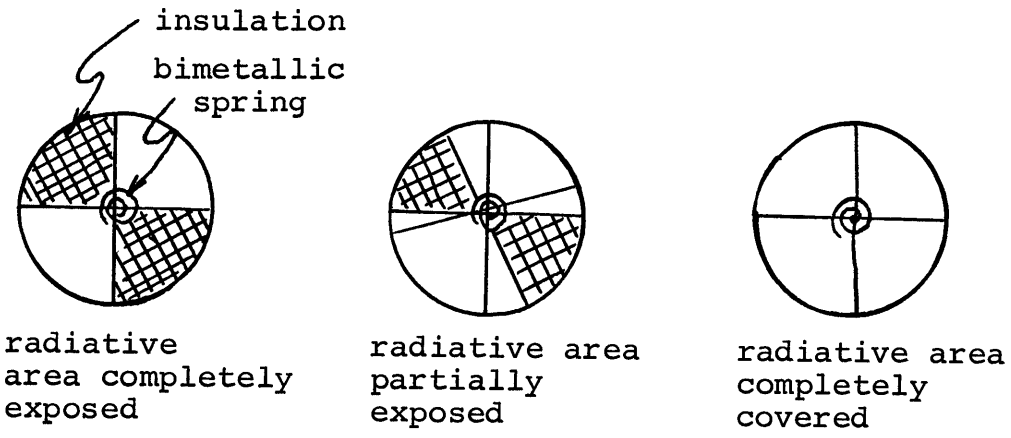

Figure 5.3 - Variable Area Mechanism Using Bimetallic Spring

Another way of changing the radiative area of the primary surface is to manually remove or replace insulation covers on the radiative surface in order to alter the ratio P/A. This method is limited by the amount of astronaut interaction required to insure reliable temperature control.

A fundamental limitation of all variable area surfaces is that they are only useful in increasing minimum temperatures--they cannot lower the maximum temperatures

below those incurred by simple radiative surfaces. However, by applying both the dual surface and variable area concepts to a design, the thermal performance of the configuration may be greatly improved with respect to both minimum and maximum temperatures.

5.3 Multi-characteristic Dual Surface Configurations

The purpose of this discussion is to point out ways of improving the thermal performance of dual surface configurations by using materials other than second surface mirrors for selective parts of the configuration. This discussion applies only to configurations operating under less than completely dirty conditions, since the surface characteristics for all materials are assumed to approach the uniform values of $\alpha_s = .90$ and $\varepsilon = .85$ under degraded conditions.

Consider the dual surface design of Figure 5.4. The effect of using a low emittance material for the bottom of the conical secondary is to reduce the amount of energy radiated by this surface, and increase the energy radiated by the high emittance material on the upper surface of the cone. Thus, the secondary radiates less energy to the primary surface, and the primary surface temperature decreases. In addition, the bottom surface of the secondary absorbs less lunar IR, and the overall temperature of the secondary will decrease.

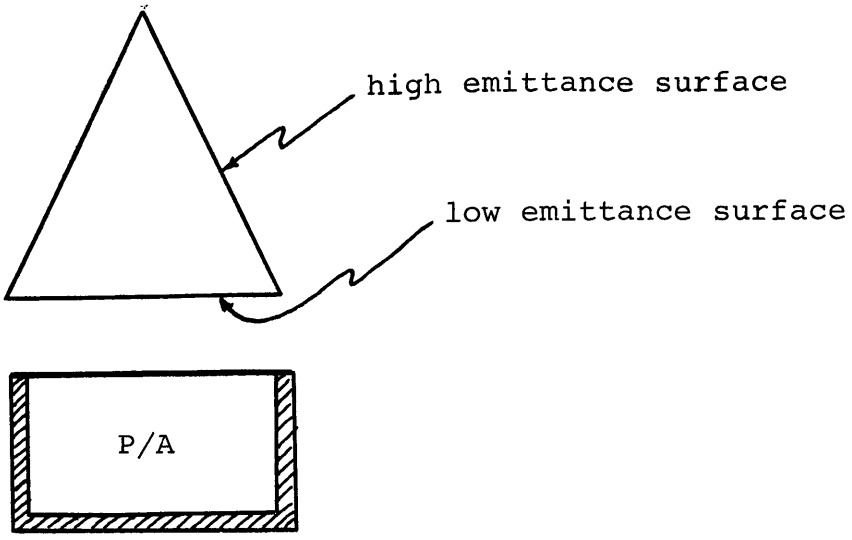

Figure 5.4 - Multi-Characteristic Secondary

However, two other effects of the low emittance surface of Figure 5.4 tend to raise the temperature of the primary surface. These effects result from reflected IR. High emittance surfaces absorb a large fraction of incident IR, but the low emittance surface of Figure 5.4 will reflect a large fraction of IR originating from the lunar and primary surfaces. Thus, the decrease in radiated energy to the primary may be offset by the increase in reflected energy, unless the design is altered.

Figure 5.5 shows a possible design modification of

Figure 5.4. The new design reflects all IR from the primary surface away from the configuration. Some lunar IR will still be reflected to the primary surface, but a large fraction of it will be reflected out of the configuration without being absorbed by the primary surface.

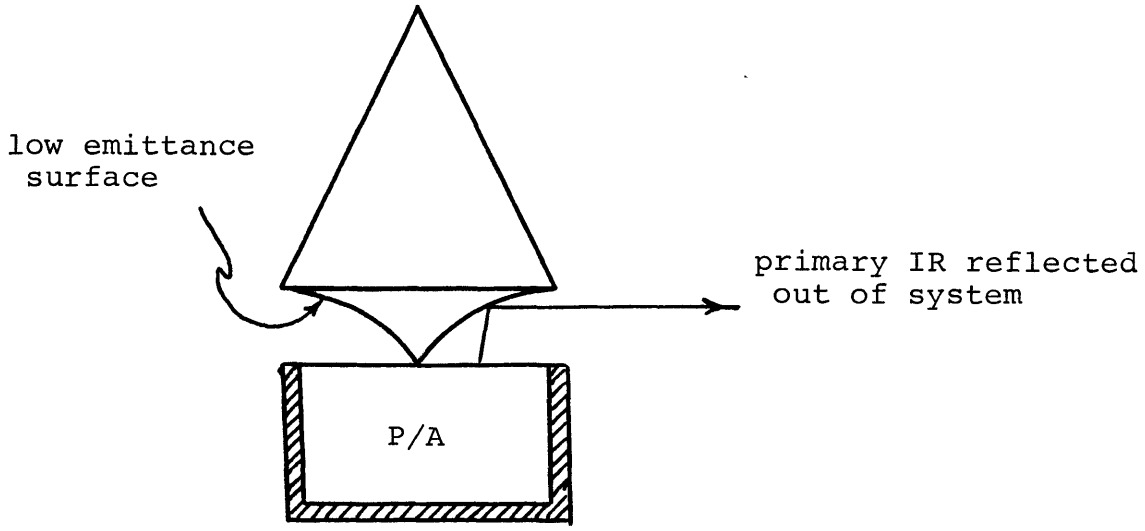

Figure 5.5 - Modified Geometry of Multi-Characteristic Secondary

Another method of lowering the temperature of the secondary surface (and thus the primary) is to reduce the absorption of lunar IR by the secondary. It is not desirable to reduce the emittance of the sides of the cone since this would cause the secondary temperature to rise, thus increasing the amount of IR radiated to the primary surface. Instead, it is possible to "block" the lunar IR

using multi-characteristic shields, as shown in Figure 5.6 The upper surface of the shield has high absorptance to reduce the amount of solar energy reflected to the secondary, and low emittance to reduce the IR energy radiated to the secondary. The bottom surface has high emittance so that a high percentage of the energy absorbed by the shield is radiated downward--away from the secondary. Again, it is important to note that these refinements are possible only if the surfaces do not become completely degraded. However, until the surfaces are <u>completely</u> degraded, i.e. α_s = .90, ε = .85, multi-characteristic materials will provide some advantage over single property materials.

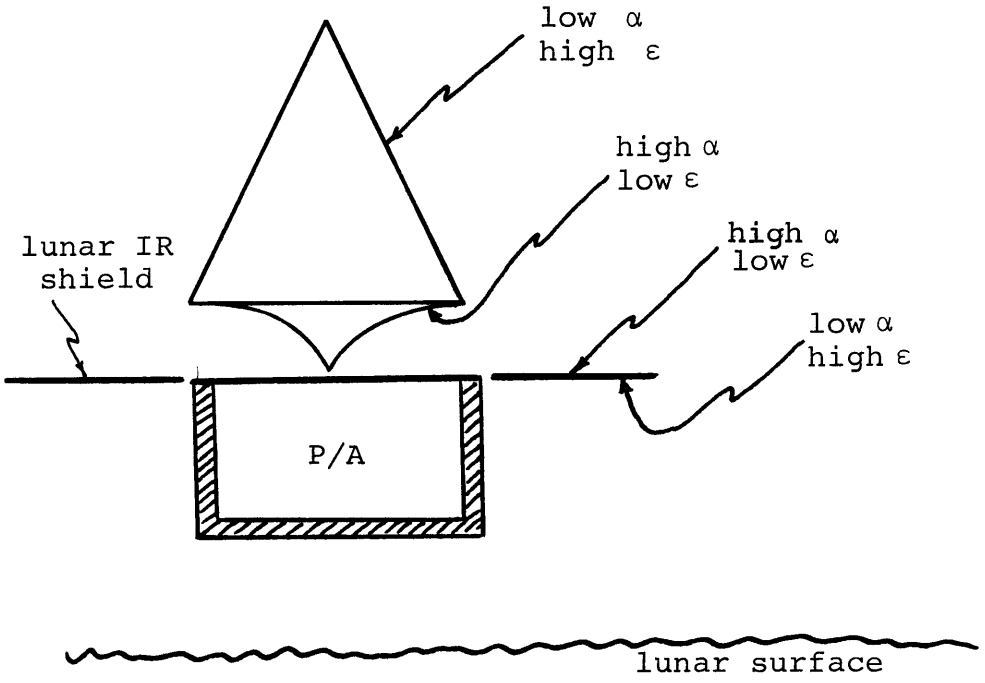

Figure 5.6 - Lunar IR Shields Using Multi-Characteristic Materials

5.4 Glass Surfaces

The use of transparent materials to improve dual surface performance is a logical extension of the preceeding discussion of multi-characteristic materials. The basic mechanism that enables multi-characteristic materials to improve thermal performance is the spectrally dependent nature of absorptance (α_s) and emittance (ε). Emittance is primarily in the infrared region, while absorptance is usually understood to refer to solar absorptance, which is primarily in the visible light spectrum.

Common types of glass are also spectrally dependent. Typically, glass is highly transparent ($\tau_V \approx .90$) to visible light, but nearly opaque to infrared radiation ($\tau_{IR} \approx .05$). In addition, glass is a good insulator--especially if thermal "sandwich" glass is considered. Figure 5.7 shows the application of glass as a lunar IR shield. It is superior to a metallic IR shield in its ability to limit IR incident on the secondary surface because it absorbs less energy. Under dirty conditions the performance of metallic and glass shields is the same.

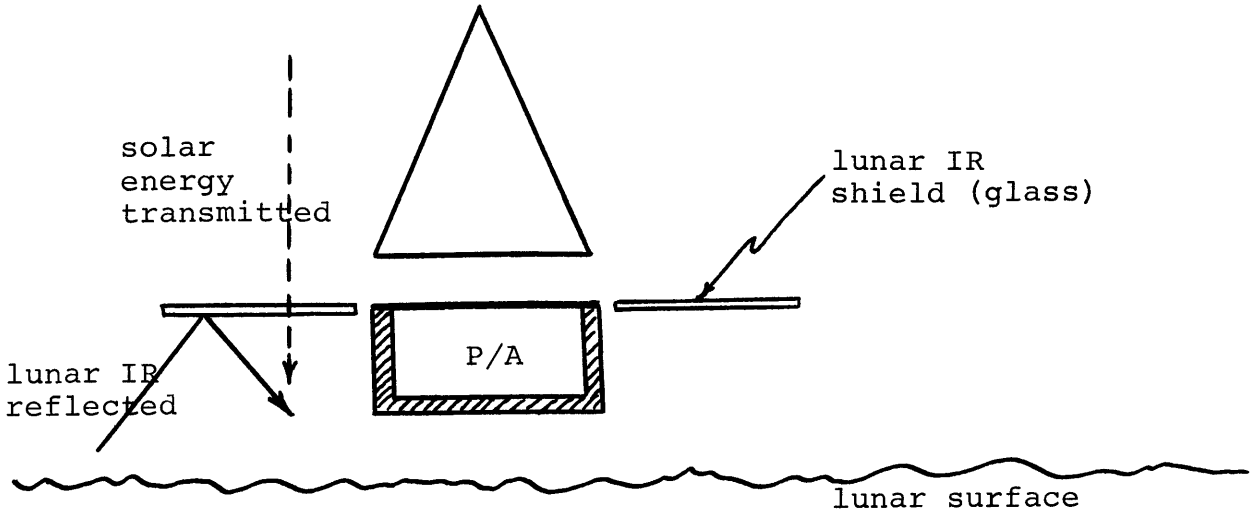

Figure 5.7 - Glass Used as a Lunar IR Shield

Glass also offers several interesting possibilities for raising minimum temperatures of the primary surface more efficiently than solar powered heaters. For instance, consider the design of Figure 5.8.

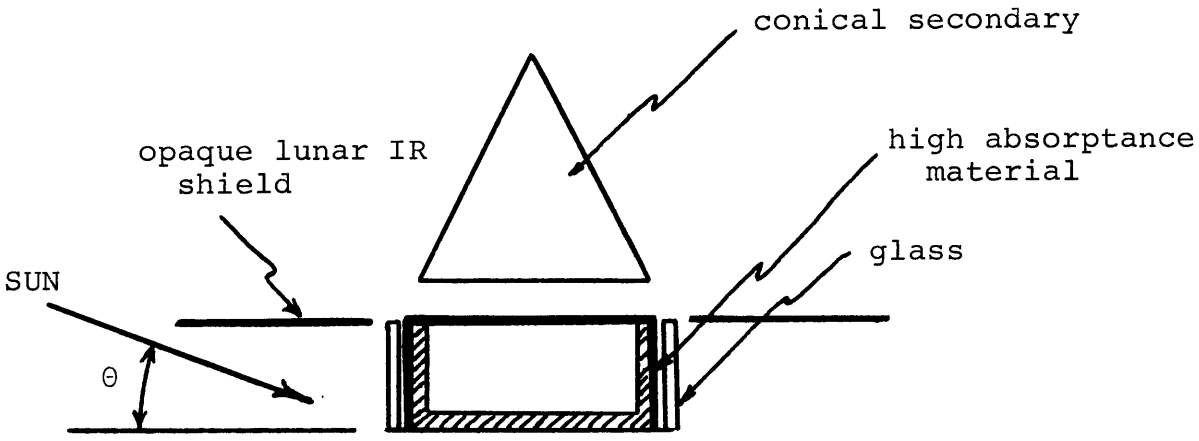

Figure 5.8 - Passive Heater Design Using Glass Covered Absorbing Surface

The design is very similar to example #6 (Figure 5.1), which demonstrated the use of a solar powered heater. In this particular case, the glass acts as an insulator and as an IR reflector. At low solar elevations, under clean conditions the glass transmits solar energy directly to the extended portion of the primary surface, thus heating the configuration. As the sun rises, the extended absorbing area becomes shaded by the opaque lunar IR shield and the glass reflects lunar IR. Since the glass acts as a good insulator, the ratio P/A is not dependent on the area of the extended absorbing surface in any way.

Under dirty conditions at high solar elevations, the surface of the glass becomes highly absorptive and emissive and absorbs lunar IR, but very little energy is transmitted to the underlying surface because the glass serves as a good insulator. Thus, maximum temperatures are not effected by this extension. At low solar elevations, the transmissivity of the glass becomes zero under dirty conditions, and no solar energy is transmitted to the extended primary surface. However, the conical secondary absorbs sufficient energy under these conditions to maintain minimum allowable operating temperatures for the SEP experiment, as shown previously in example #5.

This method of raising minimum temperatures has significant advantages over the solar powered heater discussed in section 5.1. First, it weighs less because the efficiency of the extended absorbing surface in converting solar energy to thermal energy is approximately 80% as opposed to 10% for the solar panels. Second, since the required absorbing area is much smaller than for solar panels, it is practical to geometrically configure the design so that no thermostat is required i.e. it becomes a completely passive design. This is done as illustrated in Figure 5.8 by providing a sun shade that completely shades the extended absorbing surface at sun elevations just below the maximum temperature elevation.

CHAPTER 6

CONCLUSIONS AND RECOMMENDATIONS

1. Planar dual surface configurations improve the thermal performance of single radiative surfaces by i) raising temperatures at low solar elevations (all surface conditions), ii) lowering temperatures at high solar elevations under dirty conditions, and iii) raising temperatures at high solar elevations under clean conditions.
2. The parameter P/A may be used to raise temperatures of the primary surface to high levels by allowing the area to approach zero. Increasing the radiative area lowers minimum temperatures more than maximum temperatures.
3. For dual surface configurations, an optimum value exists for the parameter S/D_1, that minimizes the maximum temperatures incurred, and maximizes the minimum temperatures. The optimum value represents the best balance between primary surface shading and secondary IR. For P/A = 13 watt/ft^2, the optimum value is $S/D_1 = .25$.
4. There is an optimum value of the parameter D_2/D_1, but its effect is insignificant compared to that of the parameters P/A and S/D_1. For P/A = 13 watt/ft^2 and $S/D_1 = .25$, the optimum value is $D_2/D_1 = 1.1$.
5. Multi-secondary configurations, using several planar surfaces, may be used to accentuate the effect of simple dual surface designs on thermal performance. This results in higher temperatures at low solar elevations and lower temperatures

at high solar elevations. The effect at elevations for which maximum temperatures occur depends on the value of the parameter S/D_1. An optimum value of S/D_1 causes the maximum temperature to decrease a few degrees centigrade for $P/A = 13$ watt/ft^2.

6. A cylindrical secondary with H >> R raises the temperature of the primary surface at low solar elevations (all surface conditions) and lowers it at high solar elevations (degraded conditions only) relative to a planar secondary surface. In all cases the cylindrical secondary raises the maximum temperature of the primary surface relative to flat plate secondaries.
7. Conical secondaries have the same general effects as cylindrical secondaries, and for a small range of the angle β, conical secondaries reduce somewhat the maximum temperature incurred by the primary surface. A value of $\beta = 120°$ yields the lowest maximum temperature for $P/A = 13$ watt/ft^2 and represents an optimum tradeoff between absorbed solar energy and absorbed lunar IR at solar elevations for which maximum temperatures occur.
8. An electric heater, powered by solar cells, is a feasible method of raising primary surface temperatures at low solar elevations. It is possible to satisfy SEP thermal requirements for clean, dusty, and very dusty conditions using a solar powered heater in a conical dual surface configuration (Figure 5.2, Table 5.1). Under dirty conditions, the solar cells are inactive, but the conical secondary absorbs

enough solar energy to maintain minimum allowable temperatures. However, for dirty conditions, the maximum allowable temperature is exceeded, rising to a maximum of 83°C.

9. Further investigation of lunar dust contamination is needed. It would be desireable to know how much dust is required to cause a certain level of degradation and what circumstances would create such a dust environment. Also, it would be useful to determine the mechanism (electrical, chemical, etc.) that causes strong adherance of lunar dust to surfaces. This type of knowledge could lead to the design of non-degrading surfaces, simply by preventing the accumulation of dust on surfaces.
10. The ideas discussed in chapter five offer potential areas for more detailed analysis and better thermal designs. In particular, the passive heating concept using a glass covered absorbing surface, and the use of multi-characteristic surfaces appear very practical.
11. A dual surface configuration using multi-characteristic materials, with a conical secondary surface, lunar IR shields, and a glass covered absorbing surface, appears to be the best approach toward satisfying SEP thermal requirements. Such a configuration would perform better than example #6, which satisfied SEP requirements for clean, dusty, and very dusty surface conditions.

APPENDIX A

UNSHADED AREA OF THE PRIMARY SURFACE

Objective

The objective of this appendix is to derive a general formulation for the exposed area of a circular primary surface when shaded by a circular secondary surface at varying solar elevations. Figure A.1 shows a side view of the basic dual surface model, with the notation to be used in this derivation.

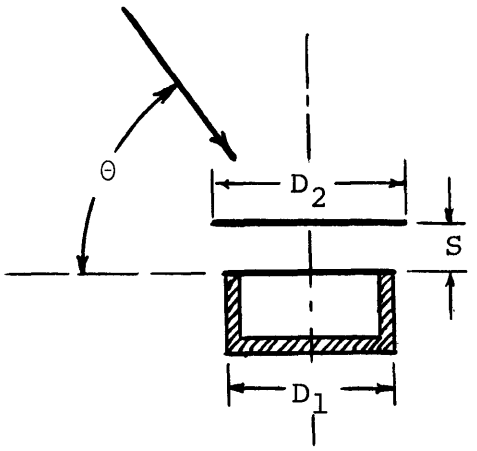

$$R_1 = \frac{1}{2}D_1$$

$$R_2 = \frac{1}{2}D_2$$

Figure A.1 - Side View of Dual Surface Model

Procedure

Figure A.2 shows the apparent displacement of secondary and primary surfaces due to solar elevation. From this figure,

$$R_1^2 = x^2 + (y + L)^2 \qquad (A.1)$$

$$R_2^2 = x^2 + y^2 \qquad (A.2)$$

and solving for the y coordinate of point P,

$$y = \frac{R_1^2 - R_2^2 - L^2}{2L} \qquad (A.3)$$

where R_1 = radius of the primary surface

R_2 = radius of the secondary surface

Θ_1 = angle defing segment one

Θ_2 = angle defing segment two

L = apparent displacement of the center of the two surfaces

$L = S \cot(\Theta)$

A_x = the exposed area of the primary surface

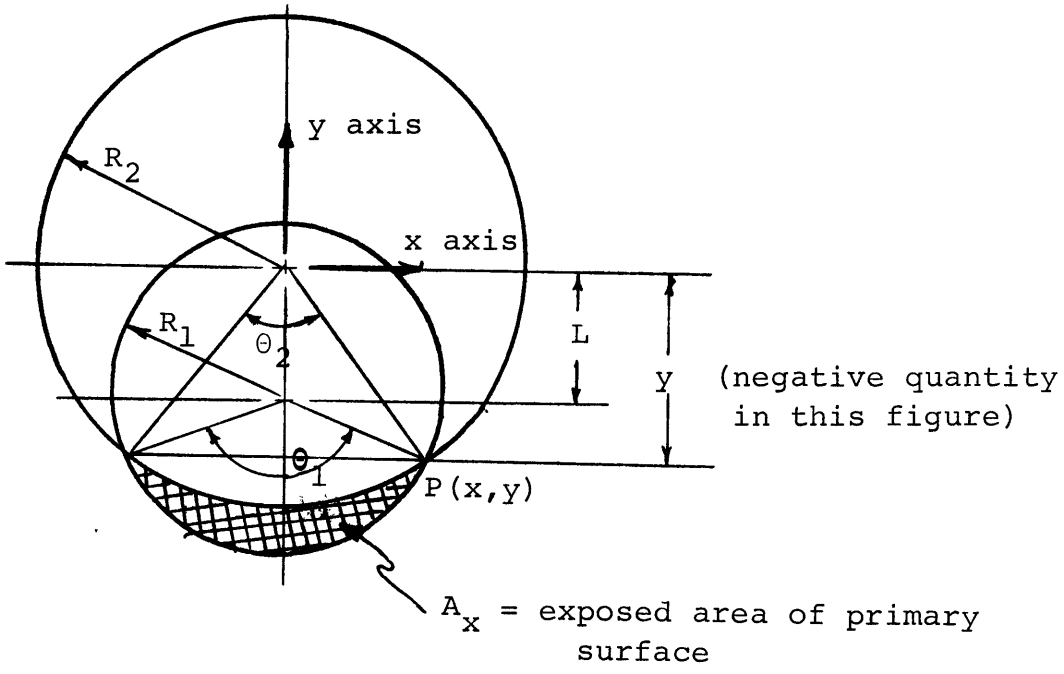

Figure A.2 - Apparent Displacement of Secondary and Primary Surfaces

Figure A.3 shows the breakdown of A_x into two segments for purposes of calculation.

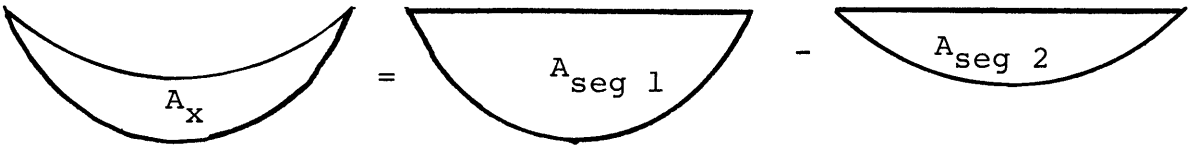

Figure A.3 - Breakdown of A_x into Segments

Calculation of $A_{seg\ 1}$, $A_{seg\ 2}$, A_x

From Figure A.3

$$A_x = A_{seg\ 1} - A_{seg\ 2} \qquad (A.4)$$

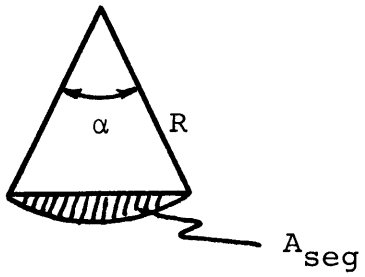

Figure A.4 - Area of a Segment

From Figure A.4, the area of a segment (A_{seg}) is given by

$$A_{seg} = \frac{\alpha}{2\pi} \pi R^2 - 1/2R^2 \sin(\alpha) \qquad (A.5)$$

Segments $A_{seg\ 1}$ and $A_{seg\ 2}$ can be calculated from equation (A.5) as shown below.

$$A_{seg\ 2} = \frac{\pi R_2^2 \theta_2}{2\pi} + xy$$

$$A_{seg\ 2} = \frac{R_2^2 \theta_2}{2} + xy \qquad (A.6)$$

where $\theta_2 = 2\mathrm{Sin}^{-1}\left(\frac{x}{R_2}\right)$

$$x = \sqrt{R_2^2 - y^2}$$

$$y = \frac{R_1^2 - R_2^2 - L^2}{2L}$$

Similarly, $A_{seg\ 1} = \frac{\pi R_1^2 \theta_1}{2\pi} + x(L + y)$

$$A_{seg\ 1} = \frac{\theta_1 R_1^2}{2} + x\ (L + y) \qquad (A.7)$$

where $\theta_1 = 2\ \mathrm{Sin}^{-1}\ \left(\frac{x}{R_1}\right)$

From Equations A.4, A.6 and A.7,

$$A_x = R_1^2 \sin^{-1}\left[\frac{R_2^2 - \frac{R_1^2 - R_2^2 - S^2\cot^2(\theta)}{2S\cot(\theta)}}{R_1}\right]$$

$$+ L\sqrt{R_2^2 - \frac{R_1^2 - R_2^2 - S^2\cot^2(\theta)}{2L}}$$

$$- R_2^2 \sin^{-1}\left[\frac{R_2^2 - \frac{R_1^2 - R_2^2 - S^2\cot^2(\theta)}{2S\cot(\theta)}}{R_1}\right]$$

APPENDIX B

EFFECTIVE ABSORBING AREA OF CONICAL SURFACES

Objective

The objective of this appendix is to obtain a general formulation for the effective absorbing area of various conical surfaces when exposed to the solar flux at solar elevations from 0^{o} to 90^{o}. Several special cases of conical surfaces are shown in Figure B.1. Derivations of area for the inverted truncated cone will be shown because this surface allows the most convenient coordinate system for analysis. Results for the non-inverted cases are similar, and will be stated but not derived. Note that the non-truncated cone may be considered a specialcase of the truncated cone, with the radius of the truncated end equal to zero, and the cylinder a special case with equal end radii.

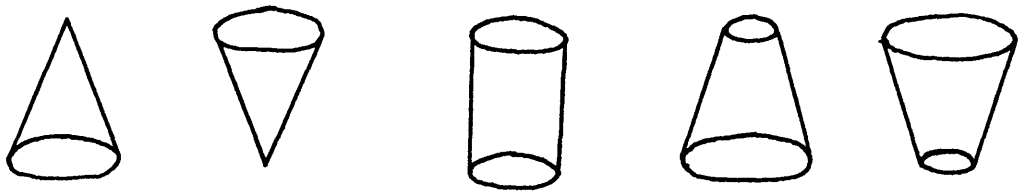

Figure B.1 - Conical Surface Considered in Appendix B

Effective absorbing area (A_{eff}) is the projected area of a conical surface exposed to direct solar flux. The area is projected in a plane normal to the solar flux. Figure B.2 shows a perspective view of the exposed area of an inverted truncated cone.

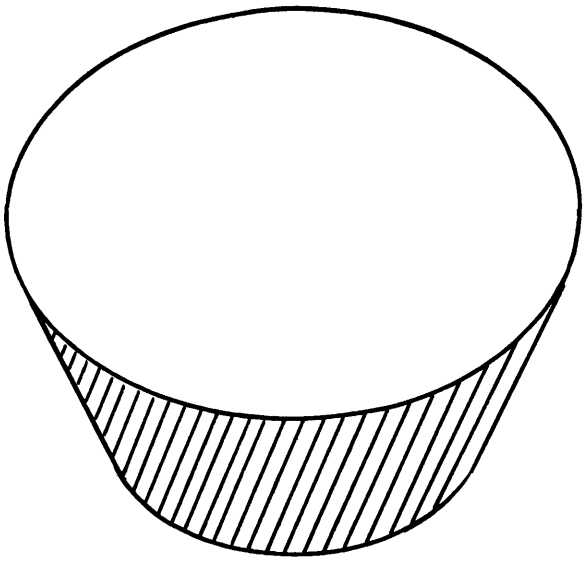

Figure B.2 - Perspective View of Absorbing Area of an Inverted Truncated Cone

Figure B.3 shows a side view of an inverted truncated cone with the notation to be used in the analysis.

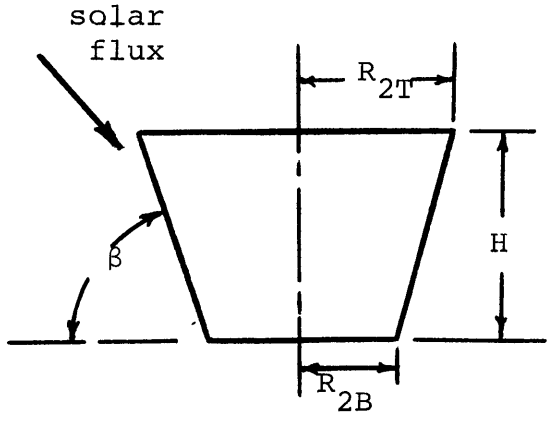

R_{2T} = radius of top of conical secondary

R_{2B} = radius of bottom of conical secondary

H = height of conical secondary

β = angle of conical side with respect to horizontal

Figure B.3 - Side View of Inverted Truncated Cone

Figure B.4 shows the area projected into a plane normal to the solar flux, and set up in a coordinate system for analysis.

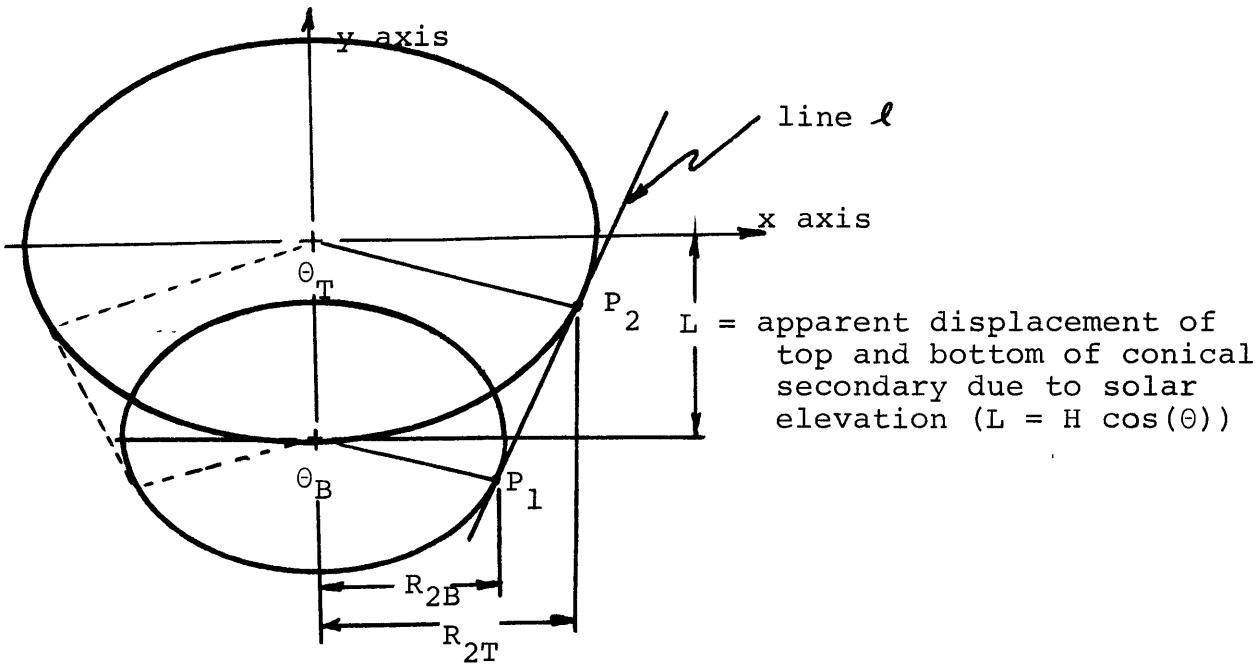

Figure B.4 - Effective Area Coordinate System

The calculation of A_{eff} may be simplified by breaking it into three segments, such that $A_{eff} = A_{trap} - A_{seg\ t} + A_{seg\ b}$ as shown in Figure B.5.

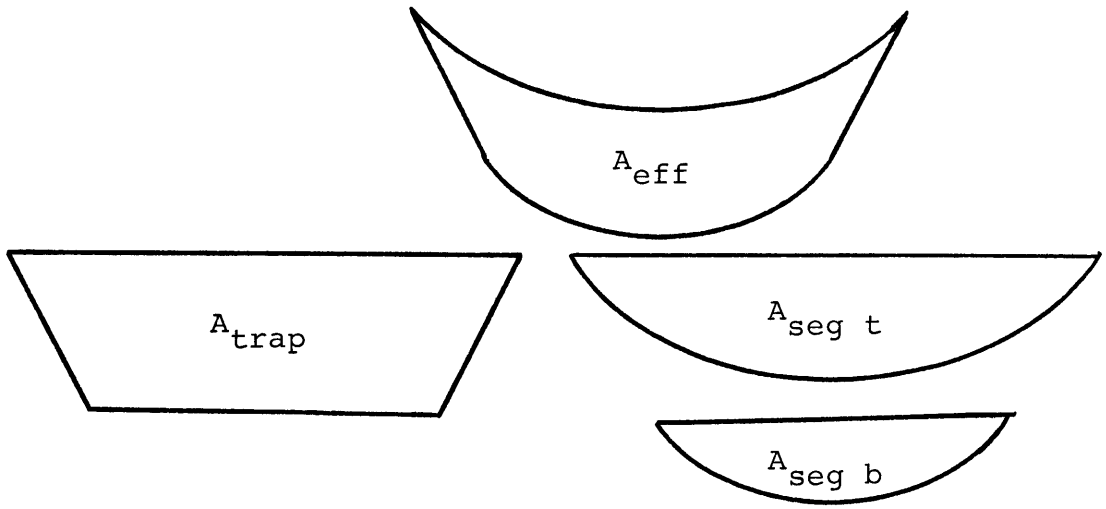

Figure B.5 - Breakdown of A_{eff} into Simpler Area

Calculation of A_{trap}, $A_{seg\ t}$, and A_{segb}

The top and bottom circular areas of a truncated cone appear as ellipses when viewed from an oblique angle. Referring to Figure B.4, the equations for top and bottom ellipses are as follows.

$$\frac{x^2}{l^2} + \frac{y^2}{\sin^2(\theta)} = R_{2T}^2 \qquad \text{(top ellipse)} \qquad \text{(B.1)}$$

$$y = -\sin(\theta)\sqrt{R_{2T}^2 - x^2} \qquad \text{(B.2)}$$

(negative root to maintain consistency with Figure B.3; lower half of ellipse)

$$\frac{x^2}{l^2} + \frac{(y + L)^2}{\sin^2(\theta)} = R_{2B}^2 \qquad \text{(bottom ellipse)} \qquad \text{(B.3)}$$

$$y = -L - \sin(\theta)\sqrt{R_{2B}^2 - x^2} \qquad \text{(B.4)}$$

(negative root for lower half of ellipse)

Implicit differentiation of equation B.1 yields

$$\frac{dy}{dx} = \frac{-2x \sin^2(\theta)}{2y} = \frac{x \sin(\theta)}{\sqrt{R_{2T}^2 - x^2}} \qquad \text{(B.5)}$$

The coordinates of points P_1 and P_2 in Figure B.4 are

$$P_2 \equiv (x,y) = (x, -\sin(\theta)\sqrt{R_{2t}^2 - x^2})$$

$$P_1 \equiv (x',y') = (x\frac{R_{2B}}{R_{2T}}, -L - \sin(\theta)\sqrt{R_{2B}^2 - \frac{R_{2B}^2}{R_{2T}^2} x^2})$$

The slope of lin ℓ and the slope of the ellipses in Figure B.4 must be equal at points P_1 and P_2 since line ℓ is tangent at these points.

$$\frac{dy}{dx} = \frac{y - y'}{x - x'} \tag{B.6}$$

Equation B.6 may be solved for coordinates of P_2 in terms of R_{2B}, R_{2T}, Θ, and H.

$$\frac{x \sin(\Theta)}{\sqrt{R_{2T}^2 - x^2}} = \frac{-\sin(\Theta)\sqrt{R_{2T}^2 - x^2} + L + \sin(\Theta)\frac{R_{2B}}{R_{2T}}\sqrt{R_{2T}^2 - x^2}}{x - x\frac{R_{2B}}{R_{2T}}}$$

$$x = \frac{R_{2T}\sin(\Theta)}{L}\sqrt{\frac{L^2}{\sin^2(\Theta)} - R_{2B}^2 + 2R_{2B}R_{2T} - R_{2T}^2} \tag{B.7}$$

where the positive root is taken for the right hand side of the ellipse, and $L = H\cos(\Theta)$

The value of x may now be used to calculate the areas of the trapazoid and segments (see Figure B.5)

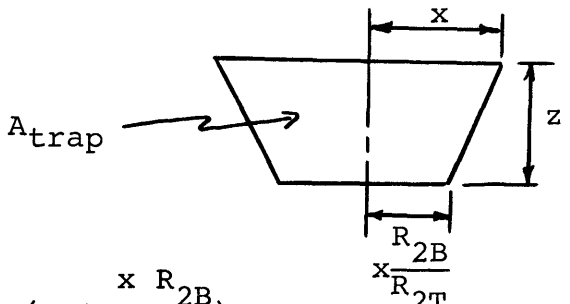

$$A_{trap} = z\left(x + \frac{x\,R_{2B}}{R_{2T}}\right) \tag{B.8}$$

where $z = (H\cos(\Theta) - R_{2T}\cos(\frac{\Theta_T}{2}) + R_{2B}\cos(\frac{\Theta_B}{2}))$

$$\text{and } \Theta_T = 2 \sin^{-1}(x/R_{2T})$$

$$\Theta_B = \Theta_T \text{ since the ellipses are geometrically similar}$$

$$A_{seg\ t} = \sin(\Theta) \left[\frac{\Theta_T}{2} R_{2T}^2 - x \cos\left(\frac{\Theta_T}{2}\right) R_{2T} \right] \qquad (B.9)$$

$$\text{for } R_{2T} \geq R_{2B}$$

$$A_{seg\ b} = \sin(\Theta) \left[\frac{\Theta_B}{2} R_{2B}^2 - x \frac{R_{2B}}{R_{2T}} \cos\left(\frac{\Theta_B}{2}\right) R_{2B} \right] \qquad (B.10)$$

$$\text{for } R_{2T} \geq R_{2B}$$

Using equations B.8, B.9, and B.10, the effective absorbing area of a cone may be calculated as

$$A_{eff} = A_{trap} - A_{seg\ t} + A_{seg\ b} \qquad (B.11)$$

For determining A_{eff} of conical surface with $\beta > \frac{\pi}{2}$ the equations for $A_{seg\ t}$ and $A_{seg\ b}$ become

$$A_{seg\ t} = \sin(\Theta) \left[\frac{(2\pi - \Theta_T)}{2} R_{2T}^2 - x \cos\left(\frac{\Theta_T}{2}\right) R_{2T} \right]$$

$$\text{for } R_{2T} < R_{2B} \qquad (B.12)$$

$$A_{seg\ b} = \sin(\Theta) \left[\frac{(2\pi - \Theta_B)}{2} R_{2B}^2 - \frac{R_{2B}}{R_{2T}} \cos\left(\frac{\Theta_B}{2}\right) R_{2B} \right]$$

$$\text{for } R_{2T} < R_{2B} \qquad (B.13)$$

REFERENCES

1. Chapman, Alan J., Heat Transfer, MacMillan Co., New York, 1967.

2. Glaser, Black, and Lindstrom, Thermal Insulation Systems, A Survey, NASA SP-5027, 1967.

3. Hamilton and Morgan, Radiant-Interchange Configuration Factors, NACA TN 2836, December 1952.

4. Krieth, Frank, Radiation Heat Transfer, for Spacecraft and Solar Power Plant Design, International Textbook Company, USA, 1962.

5. Surveyor III, A Preliminary Report, NASA SP-146, June 1967.